Communication of IUGS Geological Standards

by Shu-zhong Shen[1], Dong-xun Yuan[2], Yi-chun Zhang[3], Charles, M. Henderson[4], Quan-feng Zheng[3], Hua Zhang[3], Min Zhang[5], Yu Dai[6], Hai-peng Xu[1], Wen-qian Wang[1], Qian Li[6], Yue Wang[3], Xiang-dong Wang[1], Lin Mu[3], Jahandar Ramezani[7], Douglas H. Erwin[8], Lucia Angiolini[9], Fei-fei Zhang[1], Zhang-shuai Hou[1], Jun Chen[10], Xi-yang Zhang[11], Shu-han Zhang[1], Qiong Wu[12], Yong-xin Pan[5], Michael Stephenson[13], and Shi-long Mei[14]*

Redefinition of the Global Stratotype Section and Point (GSSP) and new Standard Auxiliary Boundary Stratotype (SABS) for the base of Wuchiapingian Stage (Lopingian Series, Permian) in South China

[1] State Key Laboratory for Mineral Deposits Research, School of Earth Sciences and Engineering and Frontiers Science Center for Critical Earth Material Cycling, Nanjing University, Nanjing 210023, China; *Corresponding author, *E-mail: szshen@nju.edu.cn*
[2] School of Resources and Geosciences, China University of Mining and Technology, Xuzhou 221116, China
[3] State Key Laboratory of Palaeobiology and Stratigraphy, Nanjing Institute of Geology and Palaeontology, Chinese Academy of Sciences, Nanjing 210008, China
[4] Department of Geoscience, University of Calgary, Calgary, AB T2N 1N4, Canada
[5] Chinese Academy of Sciences (CAS) Key Laboratory of Earth and Planetary Physics, Institute of Geology and Geophysics, Chinese Academy of Sciences, Beijing 100029, China
[6] Guangxi Institute of Regional Geological Survey, 6 Huanchengnaner Road, Guilin, Guangxi 541003, China
[7] Department of Earth, Atmospheric and Planetary Sciences, Massachusetts Institute of Technology, Cambridge, MA 02139, USA
[8] Department of Paleobiology, MRC-121, National Museum of Natural History, Washington, D.C. 20013-7012, USA
[9] Dipartimento di Scienze della Terra "Ardito Desio", Università degli Studi di Milano, Via Mangiagalli 34, I-20133 Milano
[10] State Key Laboratory of Isotope Geochemistry and CAS Center for Excellence in Deep Earth Science, Guangzhou Institute of Geochemistry, Chinese Academy of Sciences, Guangzhou 510640, China
[11] Key Laboratory of Ocean and Marginal Sea Geology, South China Sea Institute of Oceanology, Innovation Academy of South China Sea Ecology and Environmental Engineering, Chinese Academy of Sciences, Guangzhou 510301, China
[12] Southern Marine Science and Engineering Guangdong Laboratory (Guangzhou), Guangzhou 511458, China
[13] British Geological Survey, Keyworth, Nottingham NG12 5GG, UK
[14] Alberta Geological Survey, 98 Avenue Edmonton, Alberta T6B 2X3, Canada

(Received: August 16, 2023; Revised accepted: September 20, 2023)

https://doi.org/10.18814/epiiugs/2023/023023

The Global Stratotype Section and Point (GSSP) of the base-Wuchiapingian Stage was formally ratified at the Penglaitan section in South China in 2005. However, the riverside GSSP section at Penglaitan and its auxiliary section at Tieqiao have been permanently flooded since 2020. We herein designate an excavated section at Penglaitan as the new GSSP and the Fengshan section as a new Standard Auxiliary Boundary Stratotype (SABS). In addition, we revised the original definition based on a detailed restudy of the conodont succession from the two sections. We define the GSSP of the base-Wuchiapingian by the First Appearance Datum (FAD) of Clarkina postbitteri *within the lineage* Jinogondolella granti → Clarkina postbitteri → C. dukouensis*. It represents a major evolutionary turnover in conodonts from* Jinogondolella *to* Clarkina *and marks the end-Guadalupian extinction event. The U-Pb date of 259.51 ± 0.21 Ma from the uppermost part of the Emeishan basalt is adopted for the GLB age. $\delta^{13}C_{carb}$ chemostratigraphy at the SABS exhibits several excursions between 3‰ and 5‰ across the GLB interval. Carbonate $^{87}Sr/^{86}Sr$ ratio is 0.707244 at the GLB. Remarkably, the SABS contains six normal and six reverse geomagnetic polarity zones in the uppermost Capitanian and three in the lowest Wuchiapingian.*

Introduction

The Lopingian Epoch is the last epoch of the Permian Period of the Paleozoic Era and has been widely documented as one of the most critical intervals in terms of biological and geological evolution of the

Earth (Erwin, 2006). The base of the Lopingian Series (also the top of the Guadalupian) recorded one of the largest marine regressions of the Phanerozoic (Haq and Schutter, 2008). Massive volcanism associated with the Emeishan igneous province (He et al., 2007; Chen and Xu, 2019) and a pre-Lopingian biotic crisis (Jin, 1993; Jin et al., 1994) or end-Guadalupian mass extinction (Stanley and Yang, 1994; Shen and Shi, 2009; Wignall et al., 2009) characterize this boundary. The Global Stratotype Section and Point (GSSP) for the Guadalupian/Lopingian boundary (GLB) was originally defined by the first appearance datum (FAD) of the conodont *Clarkina postbitteri postbitteri* within the lineage *Jinogondolella granti*→*Clarkina postbitteri hongshuiensis*→*C. postbitteri postbitteri*→*C. dukouensis* at the base of Bed 6k of the

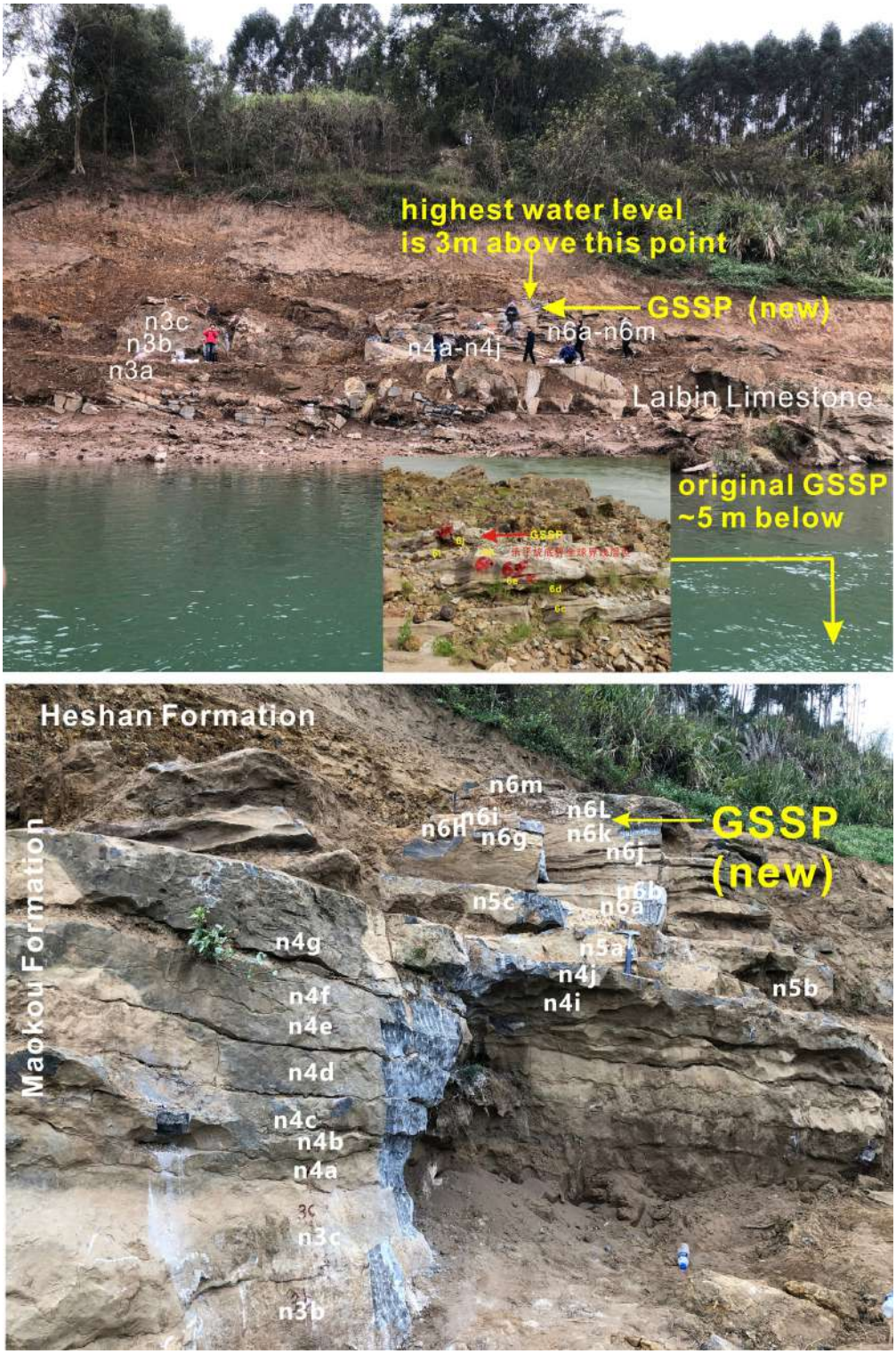

Figure 1. Photos showing the normal water level of the Hongshui River and the new section with the newly defined GSSP. All bed numbers are prefixed with "n" to differentiate from those of the original GSSP section under water.

Penglaitan section in the Laibin area of Guangxi Province (Jin et al., 2006). This base-Lopingian GSSP was formally ratified on September 3, 2005 by the International Commission on Stratigraphy (ICS) of the International Union of Geological Sciences (IUGS). It has been well protected by the local Laibin Government of Guangxi Province, and two monuments were established after the GSSP was formally ratified.

The GSSP section (23°41′43″, 109°19′16″) (Fig. 1A) cropped out along the southern bank of the Hongshui River at Penglaitan, about 13 km southeast to the Laibin City in Guangxi and was easily accessible in most seasons of the year except during the summer flooding. The Hongshui River is one of the main tributaries of the Pearl River in the Guangxi Province of South China. A dam with a hydroelectric station for protecting tens of millions of people from periodic flooding was constructed 80 km downstream from the GSSP section during the past six years. Filling the dam reservoir elevated the water level in the Hongshui River by ~15 m and caused both the Penglaitan GSSP section and its auxiliary Tieqiao section near the Laibin City to be submerged permanently since 2020.

In order to remedy the accessibility problem, an international team was organized six years ago to work on the base-Lopingian GSSP and search for a replacement section. On the one hand, two boreholes were drilled intersecting the middle Wuchiapingian to the middle Guadalupian at the Penglaitan section, and a square metre trench at the original GSSP section was cut. The rock slice across the main GLB interval, which is about 50 m long, has been moved to a storage museum on the Penglai Islet near the Penglaitan section. On the other hand, the team searched for a new replacement section for the Penglaitan GSSP section since the dam had been planned a decade earlier. The new GSSP at Penglaitan and the SABS at Fengshan have been formally ratified by the ICS, IUGS and SPS in July, 2023. In this paper, we provide a detailed report for the new GSSP for the base of the Wuchiapingian Stage (also the base of the Lopingian Series) and document a Standard Auxiliary Boundary Stratotype (SABS) (Head et al., 2022) for the Guadalupian-Lopingian boundary interval at Fengshan, Liuzhou City in Guangxi, South China.

New GSSP Section and Revised Definition for the GLB at Penglaitan

New Section at Penglaitan

The river banks at Penglaitan were heavily covered by Quaternary alluvium and vegetation before the GSSP was flooded. In order to explore the presence of additional GLB strata beneath the surface, we excavated the river bank in a place about 10 m above the original GSSP. An excellent short section with the GLB interval was found (Figs. 1 and 2). The new outcrop contains the stratigraphic interval from Units 2-6 of the Laibin Limestone of the uppermost Maokou Formation to the lowest part of Unit 7 of the basal Heshan Formation. Large samples for conodonts were collected repeatedly from the Laibin Limestone and the basal part of the Heshan Formation. The Laibin Limestone at the new section is mainly composed of massive crinoid limestone, and bedding planes are difficult to trace laterally from the original GSSP point. This might be related to differential weathering. Our studies indicate that Bed n6k contains some specimens of *Jinogondolella granti* (Figs. 3.1 and 3.2) and the Bed n6L to Bed n6m contains *Clarkina postbitteri* and transitional forms between *Jinogondolella granti* and *Clarkina postbitteri*, which are more or less comparable with *C. postbitteri hongshuiensis* (e.g., Figs. 3.9-3.19). The population contains transitional forms from the morphotypes with relatively straight platform, obtusely pointed posterior margin, relatively low blade and discrete denticles on the blade (e.g., Figs. 3.11-13, 16) and the other morphotype with a wide and slightly anteriorly arched platform with a high blade and fused denticles (e.g., Figs. 3.10, and 3.17-19). The former morphotype is relatively small or immature, therefore, possesses some characters inherited from *Jinogondolella granti*; the later morphotype is relatively large and has more characters of *Clarkina postbitteri*. Thus, the lineage from *Jinogondolella granti*→*Clarkina postbitteri*→*C. dukouensis* is recovered at the new GSSP section in association with transitional forms between *Jinogondolella granti* and *Clarkina postbitteri*. The original GSSP was recognized and correlated by the FAD of the conodont *C. postbitteri postbitteri* within the lineage *Jinogondolella granti*→*Clarkina postbitteri hongshuiensis*→*C. postbitteri postbitteri*→*C. dukouensis* (Jin et al., 2006). However, transitional forms existed in the topmost part of *Jinogondolella granti* Zone and throughout the *Clarkina postbitteri* Zone, and the two subspecies could not be resolved stratigraphically at the new section in terms of sample population approach, which is about 10 m higher topographically than the original GSSP (Fig. 1). The new section is still flooded during much of the year. We therefore recommend that the GSSP for the base of the Wuchiapingian Stage is to be maintained at Penglaitan and also formally document the Fengshan section as a SABS for the GLB interval. The new GSSP section at Penglaitan and the SABS section at Fengshan are described in Appendices 1 and 2 respectively, and will be practically used for future studies of the GLB.

Revised Definition of the GLB

The base-Lopingian GSSP at the Penglaitan was previously defined at a point at the base of Bed 6k of the Laibin Limestone, which was deposited during a major lowstand associated with a widespread regression recognizable globally (Jin et al., 2006; Yuan et al., 2017). Based on the discussions above, we suggest that this GSSP is slightly modified to correspond to the base of Bed n6L at the new section at Penglaitan, which can be recognized and correlated by the FAD of *Clarkina postbitteri sensu lato* within the lineage *Jinogondoella granti* →*Clarkina postbitteri*→*C. dukouensis* (Figs. 1 and 2) (Jin et al., 2001b). In South China, a widespread unconformity caused by the Dongwu uplift and global eustatic lowstand at the GLB (Hu, 1994; Hou et al., 2020) is present and marked by the Wangpo Shale and is commonly associated with a purple limonite bed. Continuous GLB intervals with complete conodont succession are very rare and have only been documented from the Penglaitan and Tieqiao sections in the Laibin area, and the Fengshan section in the Liuzhou area of Guangxi, the Douling area in Chenzhou, Hunan Province (Mei et al., 1994b, 1998; Shen and Zhang, 2008). Therefore, there was considerable debate regarding the conodont lineage and the definition for the GLB (Jin, 2000; Wang, 2000, 2001; Jin et al., 2001a; Kozur and Wang, 2002; Henderson et al., 2002; Wardlaw and Henderson, 2002). Jin et al. (2001b) proposed two positions for the base-Lopingian GSSP: Option A was the

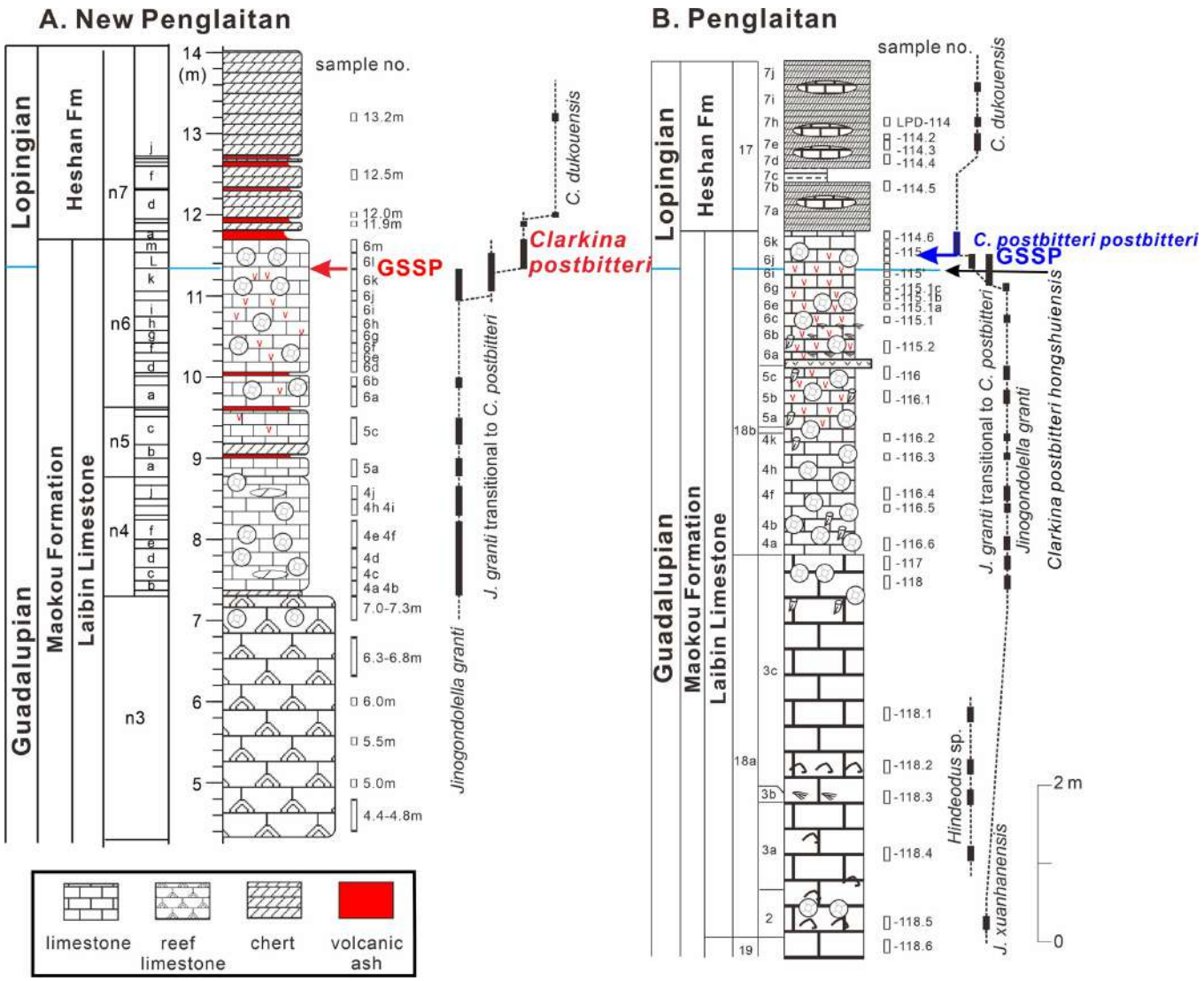

Figure 2. Correlation of conodont ranges across the Guadalupian-Lopingian boundary interval between the original and new Penglaitan sections. A, new GSSP section; B, original GSSP section (after Jin et al., 2006).

lowest occurrence of the conodont *C. postbitteri* in Bed 6i upper; Option B was the lowest occurrence of *C. dukouensis* at Bed 7e at the Penglaitan section (Fig. 2B). Option A is excellent as it represents the FAD of the conodont genus *Clarkina* globally and it has been proven that this position represents a major evolutionary changeover and the end-Guadalupian mass extinction level within the conodont lineage from the Guadalupian *Jinogondolella* to the Lopingian *Clarkina* (Henderson et al., 2002). However, this position was previously opposed by some conodont specialists who raised the questions about the ancestor of *C. postbitteri* and whether or not there is a small gap or diastem (at the bedding plane) between Beds 6i lower and 6i upper because no transitional morphotypes between *Jinogondolella granti* and its successive species *Clarkina postbitteri* were found at Penglaitan (Wang, 2000, 2001; Kozur and Wang, 2002). As a result, two subspecies of *C. postbitteri*, *C. postbitteri hongshuiensis* and *C. postbitteri postbitteri*, were separated and described (Henderson et al., 2002). The base-Lopingian GSSP was largely defined at a transitional interval between *Jinogondolella granti* and *Clarkina postbitteri* using the FAD of the conodont *C. postbitteri postbitteri* within the lineage *Jinogondolella granti→Clarkina postbitteri hongshuiensis→C. postbitteri postbitteri→C. dukouensis* (Henderson et al., 2002; Jin et al., 2006), which could be interpreted as the FAD of *Clarkina postbitteri* (*s.l.*).

Since the two subspecies to define the base-Lopingian GSSP cannot be resolved in stratigraphic order in the new Penglaitan section, we herein revert to the first definition of Jin et al. (2001b) and propose that the GSSP to be defined by the FAD of *Clarkina postbitteri* at the base of Bed n6L at the new Penglaitan section ("n" is prefixed for all bed numbers of the new section to differentiate from the original GSSP bed numbers). The main reasons for this modification are as follows. 1) The new definition represents a turning point in the evolutionary change of the Permian conodonts from the Guadalupian *Jinogondolella* to the Lopingian *Clarkina* and the end-Guadalupian mass extinction interval, and the FAD of *C. postbitteri* has been practically used for identifying the GLB as the GSSP was formally defined. The two subspecies of *C. postbitteri* (*C. postbitteri hongshuiensis* and *C. postbitteri postbitteri*) are more or less transitional (Henderson et al.,

Figure 3. Key conodonts from the new GSSP section at Penglaitan. 1-8* Jinogondolella granti*, 1, 2 from Sample n6k, 3, 4, 6-8 from Sample n5a, 5 from Sample n6j; 9-19* Clarkina postbitteri*, 9-14, 19 from Sample n6m, 15-18 from Sample n6L-n6m.

2002; Jin et al., 2006). In addition, undisputed specimens of *C. postbitteri hongshuiensis* have rarely been found elsewhere outside of Penglaitan. Although *C. postbitteri hongshuiensis* has been reported from West Texas (Lambert et al., 2002), Panthalassa (Nishikane et al., 2011),

South China (Sun and Xia, 2006; Zhang et al., 2008) and Oman (Baud et al., 2012), most of those records have since been revised and included in other species (Yuan et al., 2017; Shen et al., 2020). 2) *Clarkina postbitteri* coexists with *Jinogondolella granti* in the lower part of the *Clarkina postbitteri* Zone at both the Fengshan (see below) and the new Penglaitan sections. Some transitional forms with a relatively narrow platform and nearly parallel lateral margins between *Jinogondolella granti* and *Clarkina postbitteri postbitteri* exist in the *C. postbitteri* population at the new Penglaitan section (Figs. 3.9-3.19) (e.g., Yuan et al., 2017, figs. 4.10, 4.11). Thus, based on the stratigraphy and conodont successions (Henderson et al., 2002), the clear ancestor of *C. postbitteri* is determined to be *Jinogondolella granti* at the Penglaitan sections in South China (Henderson et al., 2002; Jin et al., 2006; Yuan et al., 2017) and the ancestor-based objection to the usage of *Clarkina postbitteri* is no longer valid. The base-Lopingian GSSP at Penglaitan was ratified nearly two decades ago, and, so far, there has been no record of *C. postbitteri* having any other lineage. 3) The FAD of *C. postbitteri* occurs at a major sequence boundary at a lowstand representing a significant global mass extinction interval at the end of the Guadalupian, therefore, it can be widely applied to different regions (Mei et al., 1999; Mei and Henderson, 2001; Shen and Shi, 2009). 4) The interval represented by the entire *C. postbitteri* Zone is narrow (less than 1 m), and a further separation of the two subspecies is difficult both taxonomically and stratigraphically everywhere else in the world.

Geochronology of the GLB

Tuffaceous beds have been documented from the bioclastic limestones of the GLB interval at the Penglaitan GSSP (e.g., Jin et al., 2001b; Jin et al., 2006). Zhong et al. (2013) studied six of these beds and concluded that they were claystones of clastic origin, as opposed to volcanic ash beds, and not suitable for geochronology. Their conclusions were based on a) mineralogy and bulk geochemistry of the rocks suggesting a clastic origin from both mafic and felsic provenances and, b) analyses of separated zircons by the LA-ICPMS (microbeam) technique showing a wide range of U-Pb ages indicative of detrital zircon. Nevertheless, three of the analyzed samples yielded major peaks in their zircon ages at ~260 Ma to ~269 Ma, which considering the large uncertainties of the analytical technique (average of ±5 Myr), tend to fall within the expected age range of the upper Guadalupian and lower Lopingian. Therefore, the possibility of acquiring meaningful depositional ages by careful zircon screening and suitable analytical methods must not be ruled out. In the newly excavated section at Penglaitan, more pronounced and well-bedded 'ash beds' have been found (Fig. 2). Samples from these beds have been collected for high-precision U-Pb geochronology by the chemical abrasion thermal ionization mass spectrometry (CA-ID-TIMS) method to be carried out at MIT, which will be published once they are available.

In the absence of radioisotopic age data directly tied to the GLB marine biostratigraphy at any location, geochronology from the Emeishan large igneous province and associated volcanic rocks in southwest China and northern Vietnam have been used as a proxy for the GLB age. With the rare exception of direct $^{40}Ar/^{39}Ar$ geochronology from basalts (Li et al., 2018), the majority of high-precision age constraints on Emeishan come from U-Pb zircon geochronology of intrusive rocks (Shellnutt et al., 2012), interlayered ignimbrites (Zhong et al., 2014), overlying rhyolites (Shellnutt et al., 2020; Huang et al., 2022) and basalt in situ paleosol horizons (red boles, see Huang et al., 2022). Tuff beds from sedimentary succession above and below the Emeishan basalts have also yielded U-Pb zircon ages (Yang et al., 2018), which place maximum and minimum age limits on the Emeishan magmatism. The bulk of reported CA-ID-TIMS geochronology constrains the Emeishan magmatism to between 259.69 ± 0.72 Ma (Ji et al., 2009) and 256.91 ± 0.77 Ma (Huang et al., 2022).

The age of GLB was initially estimated at ~259.1 Ma by Shen et al. (2010). Later, the CA-ID-TIMS U–Pb age of 259.51 ± 0.21 Ma from the uppermost tuff of the Puan volcanic sequence in the eastern Emeishan large igneous province by Yang et al. (2018) was considered the best age estimate for the GLB (Ramezani and Bowring, 2018; Shen et al., 2020; Wu et al., 2020). The latter has been adopted for the age of the GLB in the latest international Permian timescale (Shen et al., 2020), pending direct geochronology from the new Penglaitan section.

A Proposal for the Fengshan Section as a Standard Auxiliary Boundary Stratotype (SABS)

Since the new Penglaitan section for the GSSP is short and flooded during much of the year, we herein also report the Fengshan section as a Standard Auxiliary Boundary Stratotype for the GLB interval to support the GSSP of the base of the Wuchiapingian (also the base of the Lopingian Series).

Location and General Stratigraphy of the Fengshan Section

In addition to the excavation of the river bank at Penglaitan, other potential replacement and auxiliary sections have been intensively searched for during the last six years. The Fengshan section located in a low mountain area (GPS: 24°31′05″, 109°17′01″) near Fengshan Town has been extensively studied (Fig. 4A). This section is 30 km northwest to Liuzhou City and 93.3 km north to the Penglaitan GSSP section (Fig. 4). Liuzhou City is the largest industrial city of Guangxi Province. The Sanyuan Expressway passes by the Fengshan Town with multiple exits. A simple highway is available from the Fengshan Town to the section. Conodont samples were collected previously to study the base-Lopingian GSSP at the Fengshan section and the conodont *Clarkina postbitteri* was briefly reported (Mei et al., 1994b, 1998).

The Permian strata are well developed in the Fengshan area and mainly distributed in the Fengshan syncline with the central part of Lower Cretaceous purple sandy mudstone containing gypsum deposits (Fig. 5). The Permian System is fully comparable with that in the Laibin area. It comprises the Maping, Chihsia, Maokou, Heshan and Talung formations, in ascending order. The Maping Formation is composed of pale thick-bedded limestone containing abundant fusulines, and ranges from the Bashkirian (Carboniferous) to early Artinskian (Shen et al., 2019). The Chihsia Formation is composed of a coal-bearing Liangshan Member in the basal part, which represents the Chinese Longlingian Stage and approximately corresponds to the Artinskian Stage and a main dark thick-bedded limestone member with chert nodules. The main limestone member of the Chihsia Formation

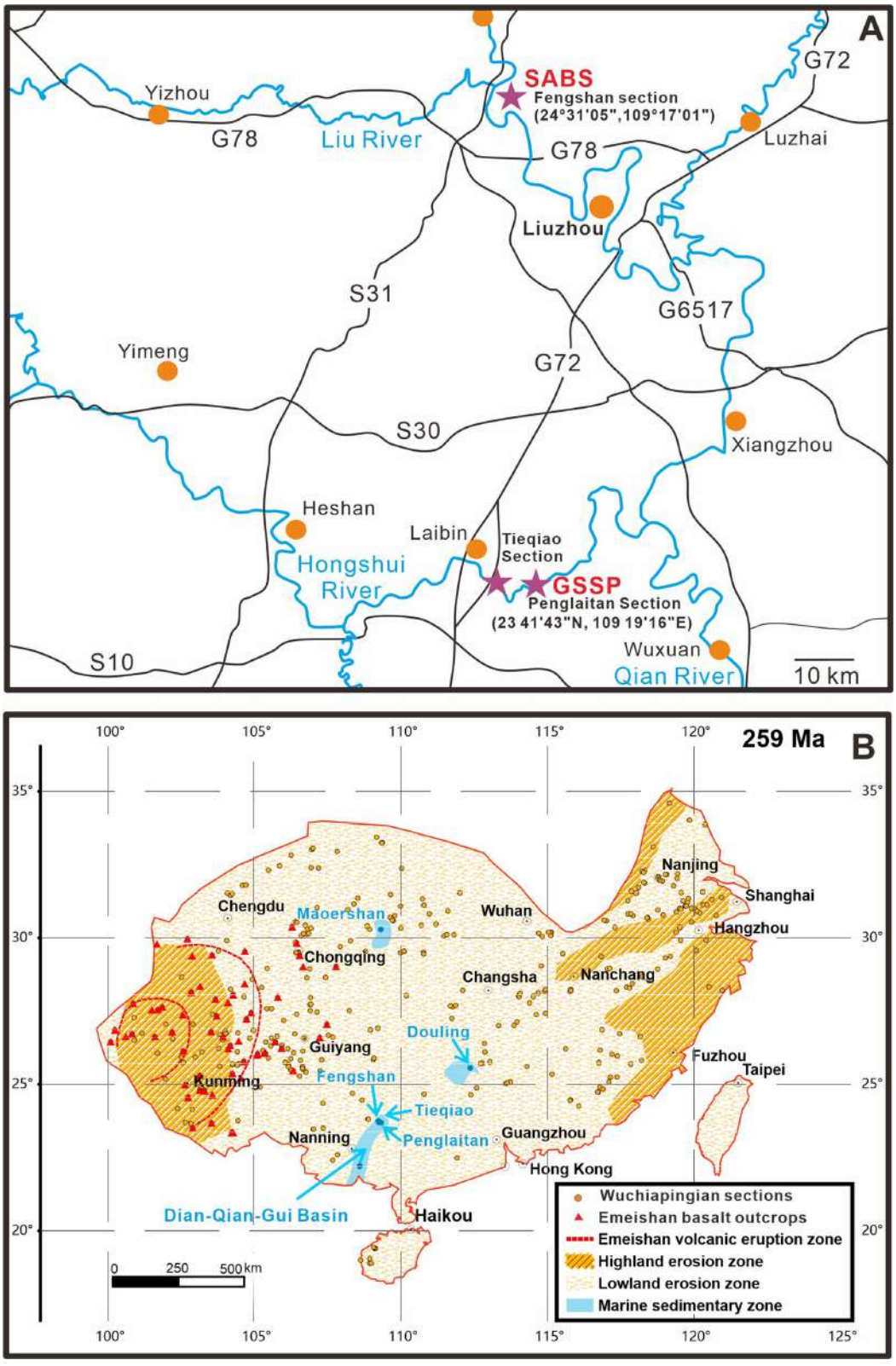

Figure 4. Map of Guangxi Province, South China showing the studied sections (A) and paleogeographical reconstruction map of the South China block during the Guadalupian/Lopingian boundary (after Hou et al., 2020) showing the locations of the Penglaitan, Tieqiao and Fengshan sections (B).

above the Liangshan Member contains abundant fusulines, rugose corals and brachiopods and mainly represents the Kungurian in South China (Sheng and Jin, 1994). This formation is composed of the most widely distributed Permian limestone basically covering the entire South China Block and it contains the same diverse marine faunas. The overlying Maokou Formation represents the Guadalupian Series

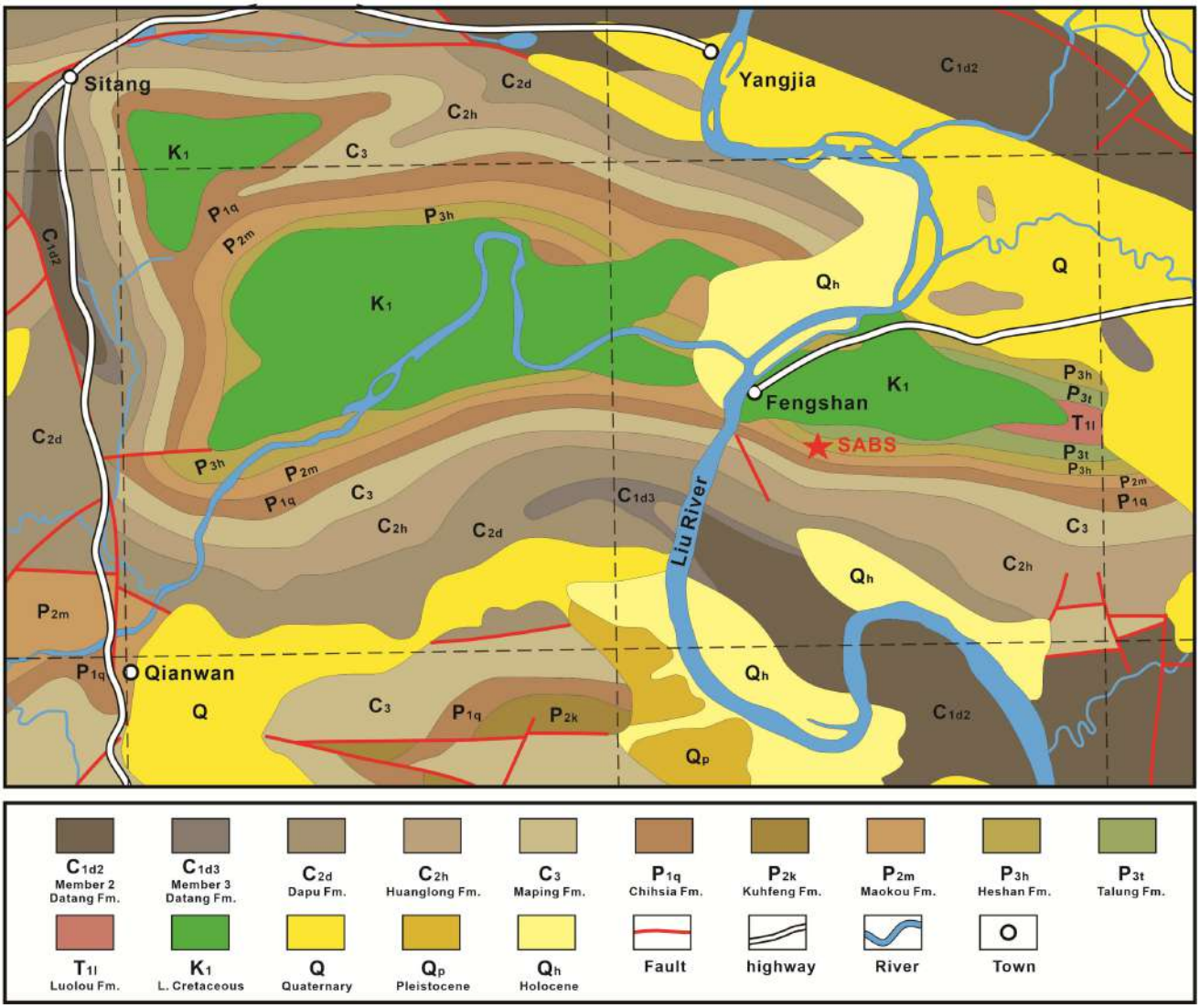

Figure 5. Geological map showing the distribution of Permian strata and the location of the SABS in the Fengshan area.

in South China, and it mainly consists of pale thick-bedded limestone containing abundant fusulines and conodonts. This formation is conformably overlain by the thin- to medium-bedded dark limestone with cherty nodules of the Heshan Formation, which is occasionally interbedded with coal beds in the studied area (Figs. 5, 6). The Guadalupian-Lopingian transition is continuous because the Fengshan section was situated in the Dian-Qian-Gui basin during the end-Guadalupian lowstand (Fig. 4B). The Heshan Formation is generally equivalent to the Wuchiaping Formation of carbonate facies and the Lungtan Formation of the coal-bearing clastic facies in South China. The uppermost Talung Formation is mainly composed of thin-bedded fragile siliceous rocks and volcanogenic tuffaceous sandstones containing abundant ammonoids, which is mostly equivalent to the Changhsing Formation of carbonate facies in South China.

Biostratigraphy of the Fengshan Section

The Fengshan section contains abundant conodonts, fusulines, brachiopods and crinoid fragments. Rare bryozoans and rugose corals have been also observed (Fig. 7).

Conodont zonation

Conodonts from the GLB interval at both Penglaitan and Fengshan sections are dominated by *Jinogondolella* in the Guadalupian and *Clarkina* in the Lopingian. Transitional morphotypes between *Jinogondolella* and *Clarkina* are present in the topmost part of the Laibin Limestone of the Maokou Formation. *Sweetognathus fengshanensis*, *Iranognathus* sp. and *Hindeodus* sp. have been commonly found. *Clarkina postbitteri* as the marker of the boundary interval from the Fengshan section has been reported in the top 0.55 m of Bed 18 of Mei et al. (1994b) and Mei et al. (1998). The complete conodont succession used for defining the base-Lopingian GSSP at Penglaitan can be found in the Fengshan section as well (Figs. 7-9).

***Jinogondolella prexuanhanensis* Zone** (-6 m ~13.3 m): This zone is not fully revealed at the measured section (Unit 0-2 to a part of Unit 17) and starts by the first occurrence of the zonal species. All the specimens are basically transitional morphotypes from *J. prexuanhanensis* to *J. xuanhanensis*. *Sweetognathus fengshanensis* is rarely found in this zone (Figs. 7, 10).

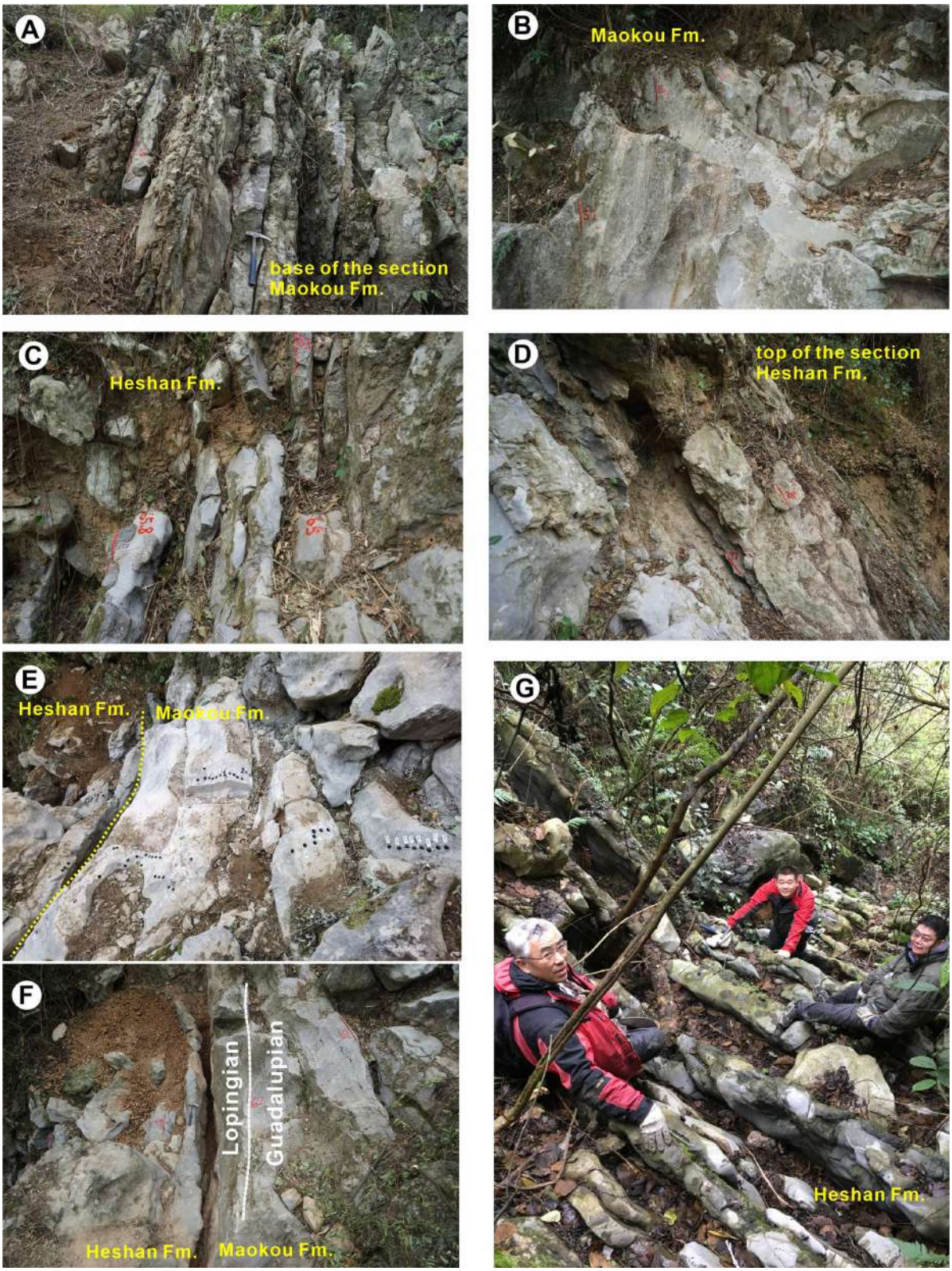

Figure 6. Outcrops of the Fengshan section (SABS) showing the lithology of the Maokou and Heshan formations. A, thin- to medium-bedded limestone with chert interbeds of the lower Maokou Formation. B, massive limestone of the upper Maokou Formation. C, D, Heshan Formation at the upper part of the section. E, F, the lithologic boundary between the Maokou and the Heshan formations and the Guadalupian/Lopingian boundary at the SABS. G, the basal part of the Heshan Formation.

***Jinogondolella xuanhanensis* Zone** (13.3 m ~ 61 m): This zone is dominated by the zonal species only, but many of the specimens are fragmentary. *Sweetognathus fengshanensis* can be found commonly in this zone. Transitional morphotypes from *Jinogondolella prexuan-*

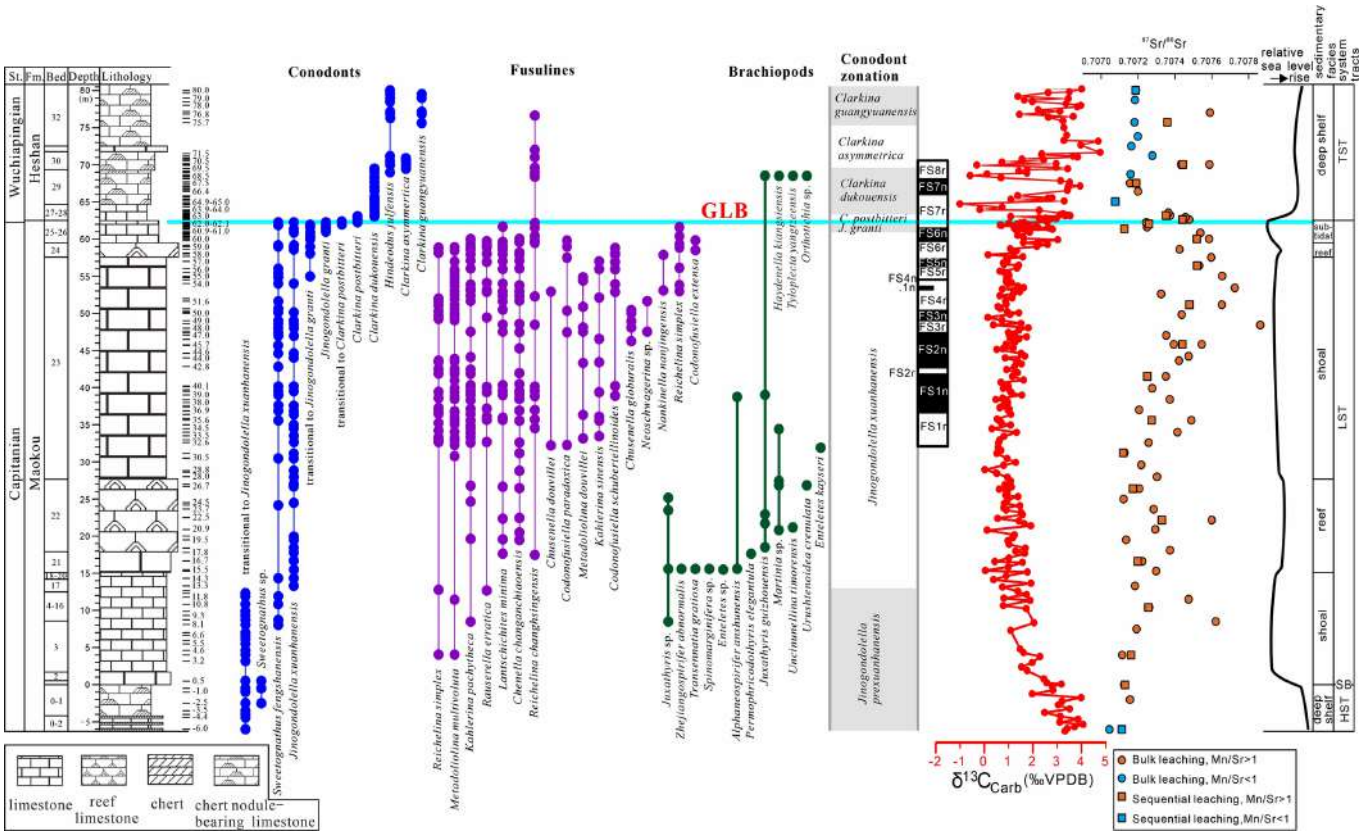

Figure 7. Stratigraphic range chart of conodont, fusuline and brachiopod fossils and $\delta^{13}C_{carb}$ and $^{87}Sr/^{86}Sr$ ratio profile of the Fengshan section (SABS).

Figure 8. The Guadalupian-Lopingian boundary interval and detailed fossil zones at the Fengshan section.

hanensis to *J. xuanhanensis* are observed from the underlying 13.3 m. In the upper part of the zone, transitional morphotypes from *J. xuanhanensis* to *J. granti* are found between Units 23-24 (27.7 m ~ 59.5 m). This zone has been widely reported from the Penglaitan section and many other sections in the world (Mei et al., 1998; Wardlaw, 2000; Lambert et al., 2002; Zhang et al., 2008) (Figs. 7, 10).

***Jinogondolella granti* Zone** (61.0 m ~ 62.0 m): This zone is found from Unit 25 and the most part of Unit 26 (61 ~ 62 m) at the Fengshan section. *J. xuanhanensis* and transitional morphotypes from *J. xuanhanensis* to *J. granti* are also commonly found in this zone. *J.*

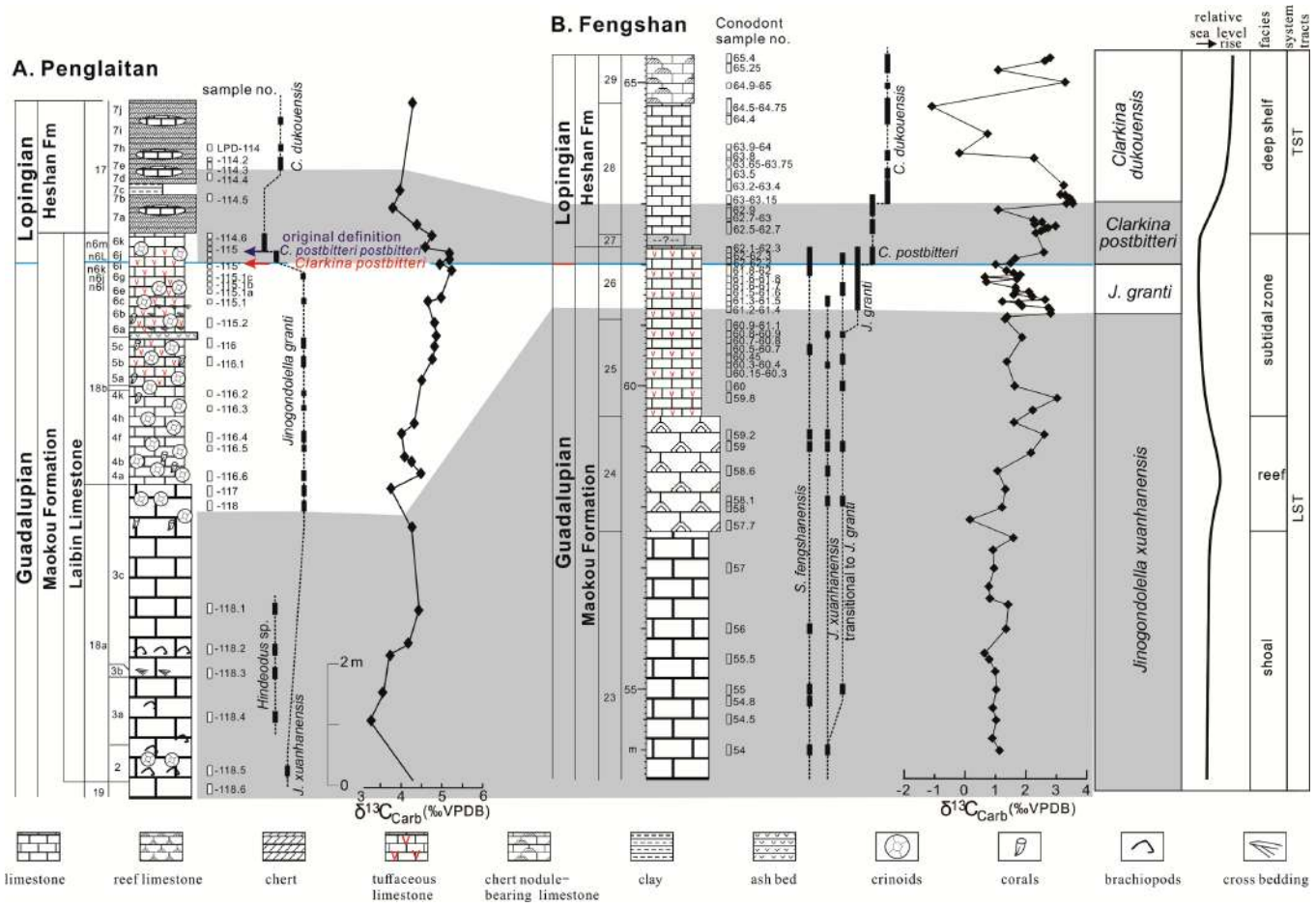

Figure 9. Correlation of fossil zones, chemostratigraphy and sedimentary settings across the Guadalupian-Lopingian boundary interval between the Penglaitan and Fengshan sections. Bed numbers with a prefix "n" are from the new section at Penglaitan. Original defined and modified GSSP are shown in the Penglaitan section.

granti ranges into the overlying *Clarkina postbitteri* Zone. *Sweetognathus fengshanensis* and *Hindeodus* sp. are also present in this zone (Figs. 7, 11).

***Clarkina postbitteri* Zone** (62.0 m ~ 63.05 m). This zone ranges across the lithologic boundary between the uppermost part (Unit 26) of the Maokou Formation and the basal part (Unit 27 and Unit 28) of the Heshan Formation. It is marked by the first occurrence of *Clarkina postbitteri*. Rare specimens of *Jinogondolella xuanhanensis* and *J. granti* continue to be present in this zone. *Sweetognathus fengshanensis* and *Hindeodus* sp. are also found. The specimens of *Clarkina postbitteri* from the uppermost part of the Maokou Formation have slightly more elongate outline and straight platform, which suggest the transitional morphotypes to *Jinogondolella granti* (e.g., Yuan et al., 2017, figs. 4.10, 4.11), therefore, more or less like *Clarkina postbitteri hongshuiensis* of Henderson et al. (2002) (e.g., Fig. 11.8). The zonal species ranges into the overlying *Clarkina dukouensis* Zone in the basal part of the Heshan Formation (Figs. 7, 11).

***Clarkina dukouensis* Zone** (63.05 m ~ 69.5 m): This zone is mainly present in dark thin- to medium-bedded limestone in the lowest part of the Heshan Formation. It is widely reported from the basal part of the Wuchiapingian Stage in South China and Iran, which was deposited during the initial stage of the widespread transgression in the Lopingian. In the basal part, *Clarkina postbitteri* is yet present. *Iranognathus* sp., *Hindeodus* sp. are also found from this zone. Some questionable specimens similar to *Clarkina asymmetrica* are also found in the middle part of the zone (Figs. 7, 12).

***Clarkina asymmetrica* Zone** (69.5 m ~ 75.7 m): This zone is marked by the first occurrence and then dominated by the zonal species. *Hindeodus julfensis* is commonly found in this zone too. In the uppermost part, some questionable specimens of *Clarkina guangyuanensis* are present. The uppermost 4.2 m (71.5 m ~ 75.7 m) has no samples, therefore, is tentatively assigned to this zone below the first occurrence of reliable *C. guangyuanensis* at 75.7 m (Figs. 7, 12).

***Clarkina guangyuanensis* Zone** (75.7 m ~ 80.0 m): This is the topmost zone at the measured section at Fengshan. It is dominated by the zonal species. *Merrilina divergens*, *Hindeodus julfensis* are occasionally found in this zone. In the upper part (79 m ~ 80 m), several questionable incomplete specimens similar to *Clarkina liangshanensis* or *C. transcaucasica* are found (Figs. 7, 12).

Fusuline zonation

In the Fengshan section, the Maokou Formation comprises thin- to thick-bedded limestone of deep shelf facies in the lower part containing the fusuline *Neoschwagerina craticulifera* Zone and the *Colania majulensis* Zone. This part is exposed on the mountains near the

Figure 10. Key conodonts from the upper part of the Maokou Formation at the Fengshan section. 1-4 **Jinogondolella prexuanhanensis** ***transitional to*** **J. xuanhanensis,** ***from Sample 12.7 m; 5-12*** **Jinogondolella xuanhanensis,** ***5 from Sample 14.3 m; 6 from Sample 17.8 m; 7 from Sample 19.5 m; 8 from Sample 34.5m; 9 from Sample 39.5m; 10 from Sample 44.6 m; 11 from Sample 47 m; 12 from Sample 50.2 m. 13-16*** **Sweetognathus fengshanensis,** ***13 from Sample 11.8 m; 14 from Sample 14.3 m; 15, 16 from Sample 40.2 m.***

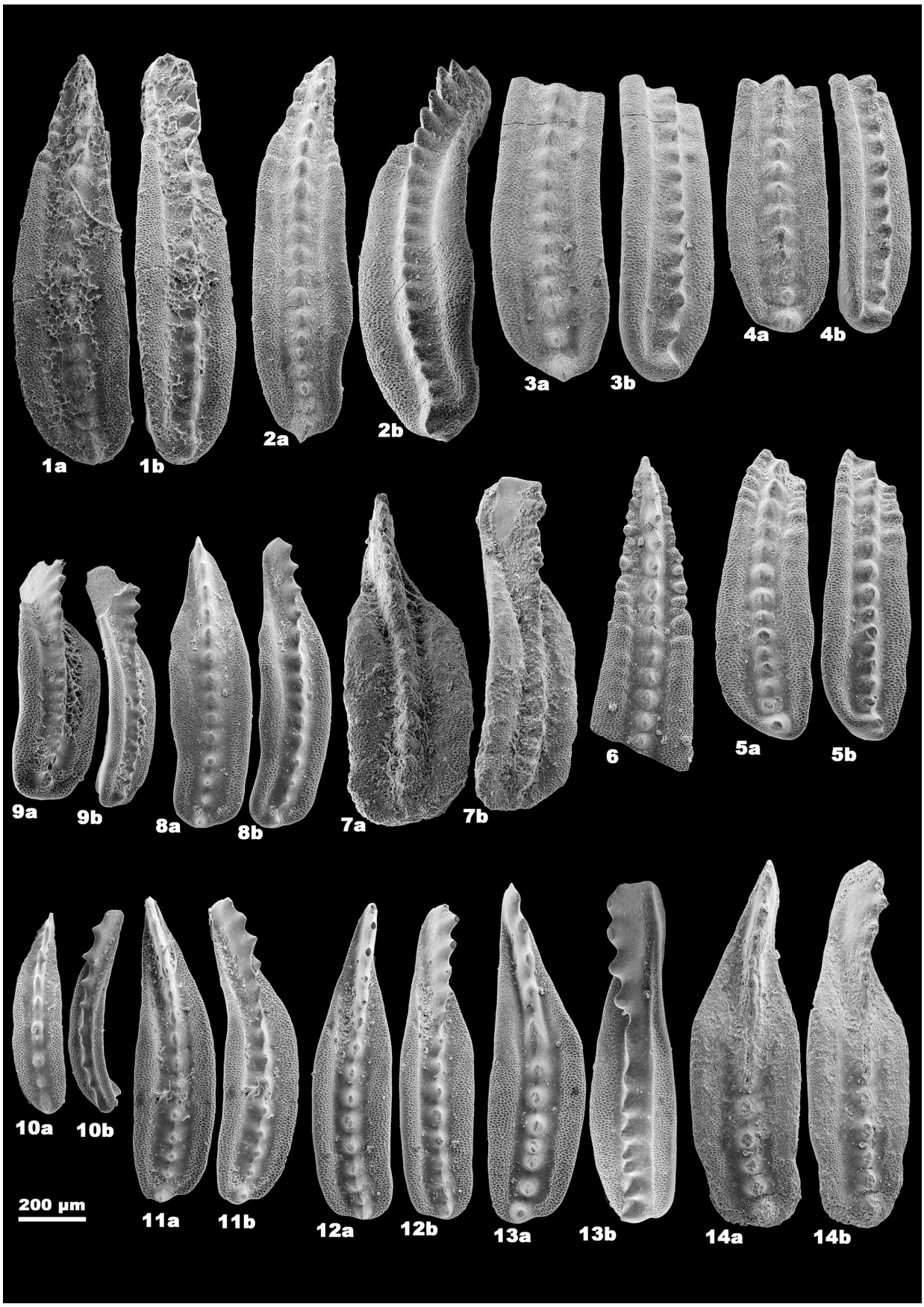

Figure 11. Key conodonts from the GLB interval at the Fengshan section. 1, **Jinogondolella xuanhanensis** ***transitional to*** **J. granti,** ***from Sample 55 m. 2-4*** **Jinogondolella granti,** ***from Sample 61.9 m. 5, 6*** **Jinogondolella** ***sp., from Sample 62.0-62.3 m. 7-9*** **Clarkina postbitteri,** ***from Sample 62.0-62.3 m. 10-14*** **Clarkina postbitteri,** ***from Sample 62.9 m.***

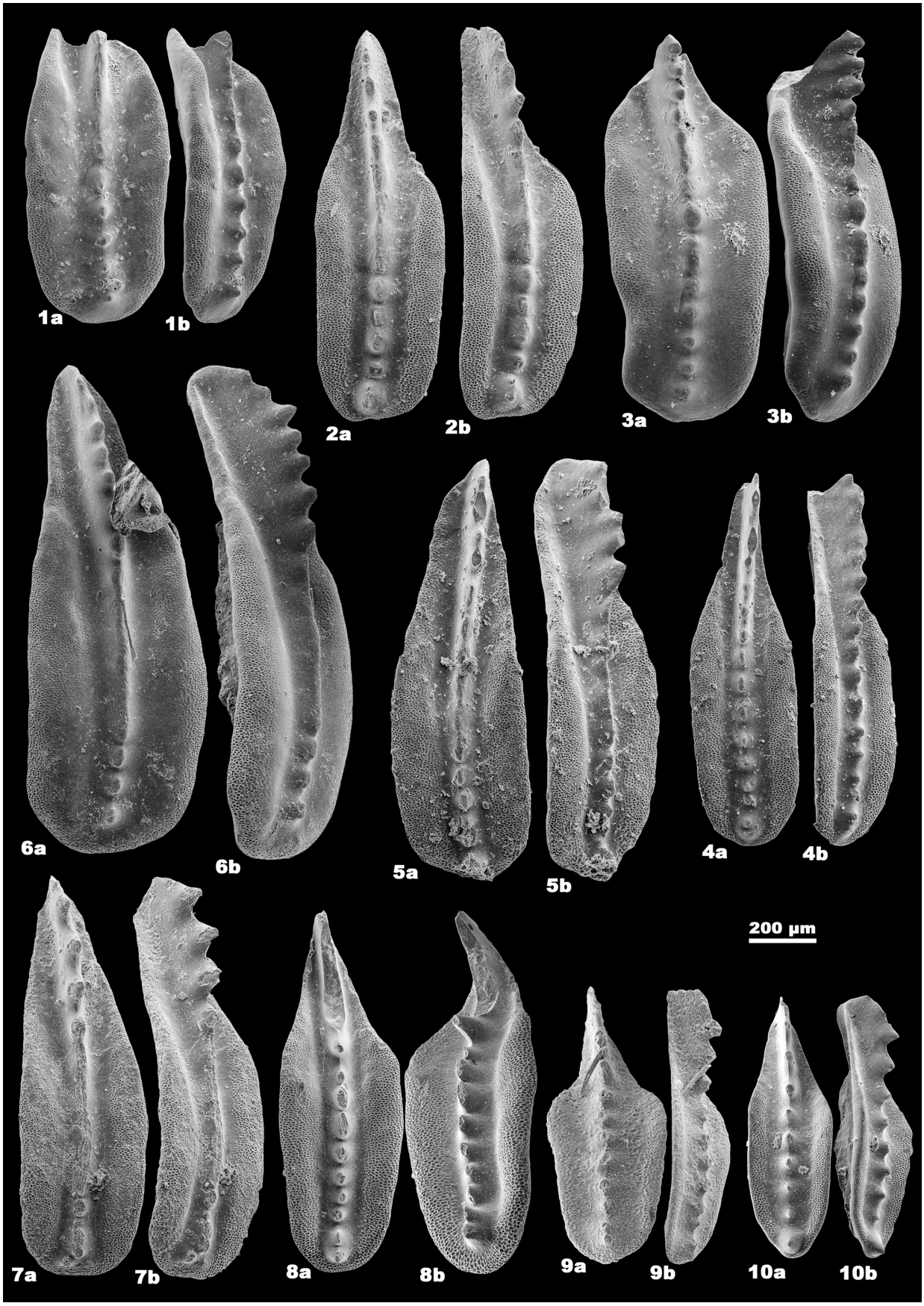

Figure 12. Key conodonts from the lower part of the Heshan Formation of the Fengshan section (SABS). 1-4 **Clarkina dukouensis**, ***1 from Sample 64.5-64.75 m; 2 from Sample 68.7 m; 3 from Sample 64.9-65.0 m; 4 from Sample 69.0 m. 5-7*** **Clarkina asymmetrica**, ***5 from Sample 69.5 m; 6 from Sample 70.5 m; 7 from Sample 70.0 m. 8-10*** **Clarkina guangyuanensis**, ***from Sample 2017-26.5 m.***

Fengshan section. The measured upper part of the Maokou Formation is composed of thick-bedded to massive sponge-bryozoan-algae bioherm limestone of platform margin facies, which is the counterpart of the Laibin Limestone at Penglaitan. The Maokouan fusulines occur in the thick-bedded bioclastic limestone very abundantly and reach about 30% of the total composition of the rock. This part contains two fusuline zones, the *Metadoliolina multivoluta* Zone in the lower and the *Lantschichites minima* Zone in the upper. *Codonofusiella* is very abundant in the uppermost part of the Maokou Formation at the Fengshan section. The overlying Heshan Formation is mainly composed of dark, thin-bedded limestone with chert beds of deep-shelf facies in the lower part and algae limestone of platform facies in the upper part and contains rare fusulines. Only one species, *Rechelina changhsingensis*, ranges from the Maokou Formation into the Heshan Formation. The widely distributed *Codonofusiella* fauna in the Wuchiapingian in South China is not found in the lowest part of Heshan Formation. The following fusuline zones can be recognized.

***Metadoliolina multivoluta* Zone** (4 m ~ 17.8 m): This zone is in the massive bioclastic limestone in the upper part of the Maokou Formation (equivalent to the Laibin Limestone) at the Fengshan section. It is dominated by *Metadoliolina multivoluta*, *M. douvillei* and *M. delicata*. Neoschwagerinids are rare and only two specimens of *Neoschwager-*

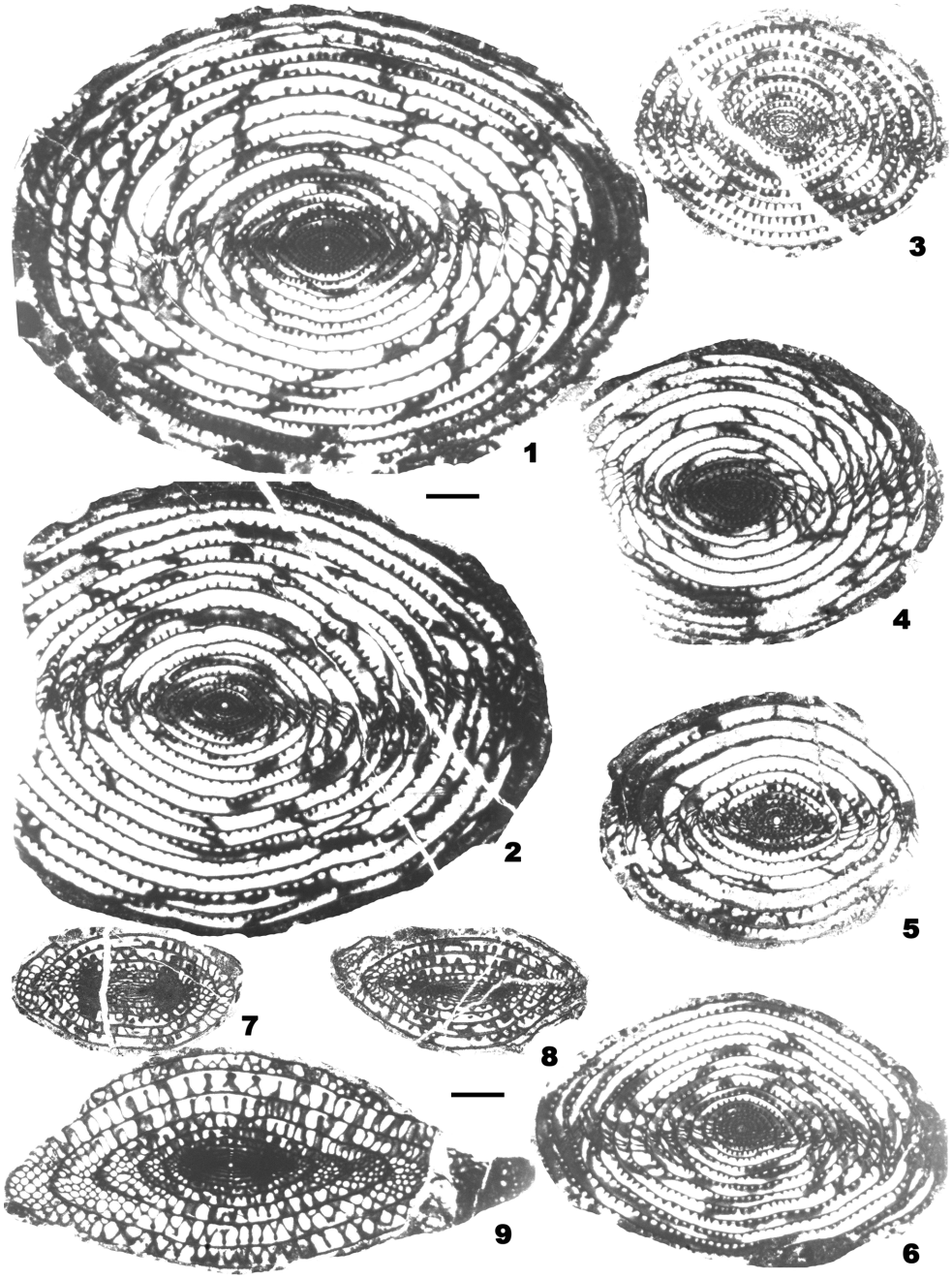

Figure 13. Fusulines from the uppermost part of the Maokou Formation of the Fengshan section (SABS). 1, 2. **Metadoliolina multivoluta** ***(Sheng, 1963). 1, 176682, axial section; 2, 176691, axial section. 3.*** **Metadoliolina douvillei** ***(Gubler, 1935), 176692, subaxial section. 4-6.*** **Metadoliolina delicata** ***(Yang, 1978). 4, 176688, axial section; 5, 176681, axial section; 6, 176690, axial section. 7, 8.*** **Chusenella douvillei** ***(Colani, 1924). 7, 176646, subaxial section; 8, 176683, subaxial section. 9.*** **Chusenella globularis** ***(Gubler, 1935), 176689, axial section. Scale bar=1 mm.***

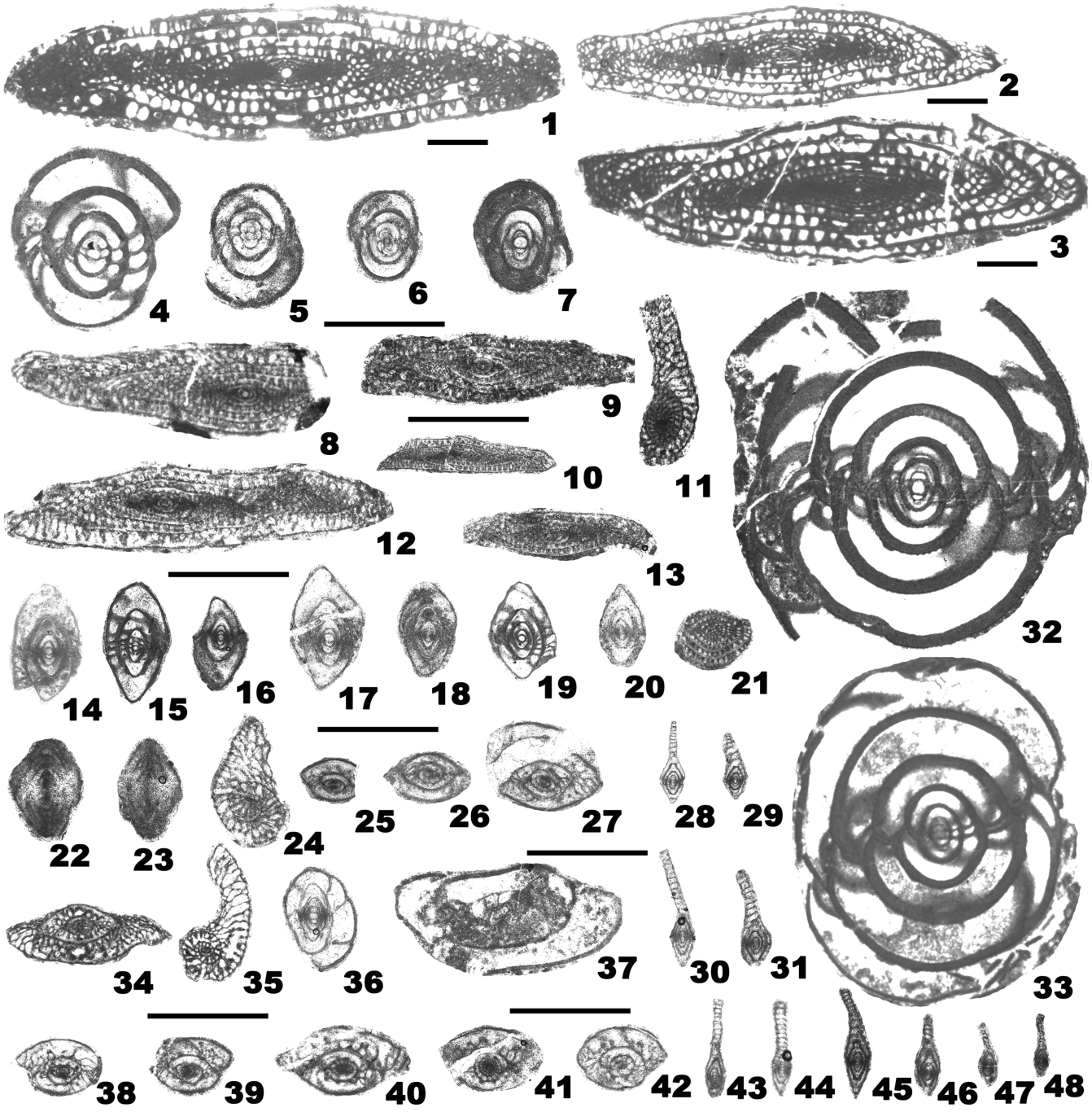

Figure 14. Fusulines from the GLB interval of the Fengshan section. 1-3. **Schwagerina serrata** ***Ding, 1978. 1, 176685, axial section; 2, 176687, subaxial section; 3, 176684, axial section. 4-7.*** **Kahlerina pachytheca** ***Kochansky-Devide and Ramovs, 1955. 4, 176668, subaxial section; 5, 176645, subaxial section; 6, 176643, axial section; 7, 176641, axial section. 8-13.*** **Lantschichites minima** ***(Chen, 1956). 8, 176639, axial section; 9, 176644, axial section; 10, 176640, subaxial section; 11, 176660, transverse section; 12, 176654, axial section; 13. 176637, subaxial section. 14-20.*** **Chenella changanchiaoensis** ***(Sheng and Wang, 1962). 14, 176667, axial section; 15, 176665, axial section; 16, 176658, axial section; 17, 176652, axial section; 18, 176653, axial section; 19, 176647, axial section; 20, 176657, axial section. 21.*** **Neoschwagerina** ***sp., 176677, oblique section. 22, 23.*** **Nankinella nanjingensis** ***Zhou and Zhang, 1984. 22, 176642, subaxial section; 23, 176655, subaxial section. 24-27.*** **Codonofusiella paradoxica** ***Dunbar and Skinner, 1937. 24, 176673, transverse section; 25, 176676, axial section; 26, 176675, axial section; 27, 176674, axial section. 28-31.*** **Reichelina simplex** ***Sheng, 1955. 28, 176662, axial section; 29, 176663, axial section; 30, 176636, axial section; 31, 176649, axial section. 32, 33.*** **Kahlerina sinensis** ***Sheng, 1963. 32, 176650, axial section; 33, 176686, axial section. 34, 35.*** **Codonofusiella extensa** ***Skinner and Wilde, 1955. 34, 176661, subaxial section; 35, 176664, transverse section. 36, 37.*** **Rauserella erratica** ***Dunbar, 1944. 36, 176656, transverse section; 37, 176638, subaxial section. 38-42.*** **Codonofusiella schubertellinoides** ***Sheng, 1956. 38, 176672, subaxial section; 39, 176670, subaxial section; 40, 176669, subaxial section; 41, 176659, axial section; 42. 176651, oblique section. 43-48.*** **Reichelina changhsingensis** ***Sheng and Chang, 1958. 43, 176679, subaxial section; 44, 176678, subaxial section; 45, 176671, axial section; 46, 176666, subaxial section; 47, 176680, axial section; 48. 176648, axial section.***

ina sp. were found in the middle part of the zone. *Chusenella globularis* and *C. douvillei* are common. (Fig. 13).

***Lantschichites minima* Zone** (17.8 m ~ 61.9 m): *Lantschichites minima* first occurs at 17.8 m in the upper part of Maokou Formation and marks the base of this zone, but it gains a dominant composition from this level until the GLB. Large *Metadoliolina* species continue to be present in the *Lantschichites minima* Zone. The disappearances of large fusulines at 58.9 m in the latest Guadalupian probably marked the profound environmental deterioration globally. Above this level, only small fusulines continue to be present. *Lantschichites minima* is commonly associated with some *Codonofusiella* species such as *C. extensa*, *C. schubertellinoides* and *C. paradoxica*. This zone is most abundant in the topmost part of the Capitanian Stage and it has been occasionally reported from the lowest part of the Wuchiapingian at the Penglaitan section in the Laibin area (Wang et al., 2020). In other regions of South China, the *Lantschichites minima* Zone is either missing or absent (Fig. 14).

Brachiopods

Brachiopods are also abundant in the interval between 8.8 m and 39 m at the Fengshan section. The brachiopod fauna is characterized by a mixed character between the upper Guadalupian and Lopingian elements (Fig. 15). In fact, the appearance of typical Lopingian brachiopod species in the Capitanian has been observed not only in sections of South China (Shen and Shi, 2009), but also in Iran (Crippa and Angiolini, 2012) and the Mediterranean region (Verna et al., 2010). The typical middle-upper Capitanian brachiopod *Urushtenoidea crenulata* is found at 27 m and a local Lengwuan (= Capitanian) species *Zhejiangospirifer abnormalis* is present at 15.5 m. *Urushtenoidea crenulata* has been widely reported from the upper part of the Capitanian and never reported from the Lopingian anywhere in the world (Shen et al., 2003; Shen and Zhang, 2008; Shen, 2018). On the other hand, some very abundant species in the Wuchiapingian in South China, Iran, Transcaucasia (Kotljar et al., 1983; Garbelli et al., 2014; Shen, 2018) including *Transennatia gratiosa*, *Permophricodothyris elegantula* and *Juxathyris guizhouensis*, are present in this interval. Therefore, this brachiopod fauna obviously indicates that the horizon is close to the latest Capitanian, which is fully comparable with that of the Penglaitan section (Shen and Shi, 2009). These are typical lower-middle Wuchiapingian taxa, which are found abundantly also in Tethyan sections (Angiolini and Carabelli, 2010; Ghaderi et al., 2014; Viaretti et al., 2022).

Chemostratigraphy

$\delta^{13}C_{carb}$ and $\delta^{18}O_{carb}$

$\delta^{13}C_{carb}$ and $\delta^{18}O_{carb}$ based on bulk samples were analyzed in order to establish the $\delta^{13}C_{carb}$ chemostratigraphy (Fig. 7). 269 bulk samples were analyzed for the 80.3 m interval across the GLB at the Fengshan section. $\delta^{13}C_{carb}$ values are between -1.09‰ and 4.76‰ with an average of 1.68‰ for the whole section. The values in the basal 4.5 m (-6 m to -1.5 m) are between 2.47-4.07‰ in the section, then declined to ~1‰ at the base of the *Jinogondolella xuanhanensis* Zone. $\delta^{13}C_{carb}$ values remain around ~1‰ through the *J. xuanhanensis* Zone until 58.3 m, then frequently fluctuated between -1.09‰ and 4.76‰ across the GLB interval. At least five negative and positive excursions are present within the interval from 58.3 m to 73 m (Figs. 7, 9). $\delta^{13}C_{carb}$ values rapidly increased from 0.16‰ at 57.3 m to 3.02‰ at 59.8 m at the base of the *J. granti* Zone. Then, $\delta^{13}C_{carb}$ values declined with two minor negative excursions of ~2‰ in the *J. granti* Zone. $\delta^{13}C_{carb}$ values bounced back to 3.53‰ at the top of the *Clarkina postbitteri* Zone, followed by another negative excursion of 4.62‰ with the lowest value -1.09‰ at 64.6 m in lower part of the *C. dukouensis* Zone. Above this negative excursion, two more negative carbon excursions with a magnitude of 4‰ respectively in the uppermost part of the *C. dukouensis* Zone and the basal part of the *C. asymmetrica* Zone are present. After that, $\delta^{13}C_{carb}$ values fluctuated between +1.44‰ and 4.67‰ (Fig. 7).

$\delta^{18}O_{carb}$ values from all bulk samples are between -9.2‰ and -4.94‰ with an average -6.69‰, therefore a diagenetic effect may be present. Moreover, the large multiple fluctuations in $\delta^{18}O_{carb}$ values around the GLB are obviously different from all other coeval sections (Fig. 7).

$^{87}Sr/^{86}Sr$ ratio

The strontium isotope ratio ($^{87}Sr/^{86}Sr$) has been widely used to date marine sediments and fossils to achieve a temporal correlation among different regions. The non-parametrical LOcally WEighted Scatterplot Smoother (LOWESS) Version 5 established with a statistical regression was widely used to interpolate the strontium isotope ratios of temporally undetermined marine sediments (McArthur et al., 2012) and it has been updated by McArthur et al. (2020). The Capitanian Stage is characterized by the Capitanian minimum with the lowest value of $^{87}Sr/^{86}Sr$ ratio between 0.7068-0.7070 in the Phanerozoic, therefore, it has been regarded as a very useful tool for correlation (Korte et al., 2006; Kani et al., 2013, 2018; Wang et al., 2018, 2021; Kani and Isozaki, 2021).

In order to investigate $^{87}Sr/^{86}Sr$ chemostratigraphy at the Fengshan section, 63 whole rock samples were collected (Fig. 7) (see Wang et al., 2018 for methdolgy).

About 10 mg of the powders were weighed for $^{87}Sr/^{86}Sr$ analyses, and a weak acid (0.2 N HAc) leaching method was used to dissolve the powders. We also tried a sequential-leaching method followed Bellefroid et al. (2018) to obtain the least-altered seawater Sr isotopic signal. Sr was extracted by cation exchange resin, and the isotopic composition was measured by Neptune-MC-ICP-MS at the Nanjing Institute of Geology and Palaeontology (NIGP), Chinese Academy of Sciences. The contents of the trace elements Mg, Fe, Mn, and Sr and the main element Ca were also analyzed to test whether these samples were altered by subsequent diagenesis or not. Major and trace elements of samples were analyzed on an Agilent 710 ICP-OES.

The results show that two leaching methods yield similar Sr isotopic trends (Fig. 7). Based on the samples with Mn/Sr < 1, a cutoff widely used for identifying diagenetic alteration (Bellefroid et al., 2018; Wang et al., 2018), the $^{87}Sr/^{86}Sr$ ratios in the Fengshan section varied from 0.707043 to 0.707276. Due to the high Mn/Sr ratios around GLB, most of the analyzed samples were considered not to represent the open marine seawater $^{87}Sr/^{86}Sr$ ratios, thus the minimum of $^{87}Sr/^{86}Sr$ ratios, a unique stratigraphic marker for the Capitanian (Liu et al., 2013; Korte and Ullmann, 2016; Li et al., 2021; Wang et al., 2021),

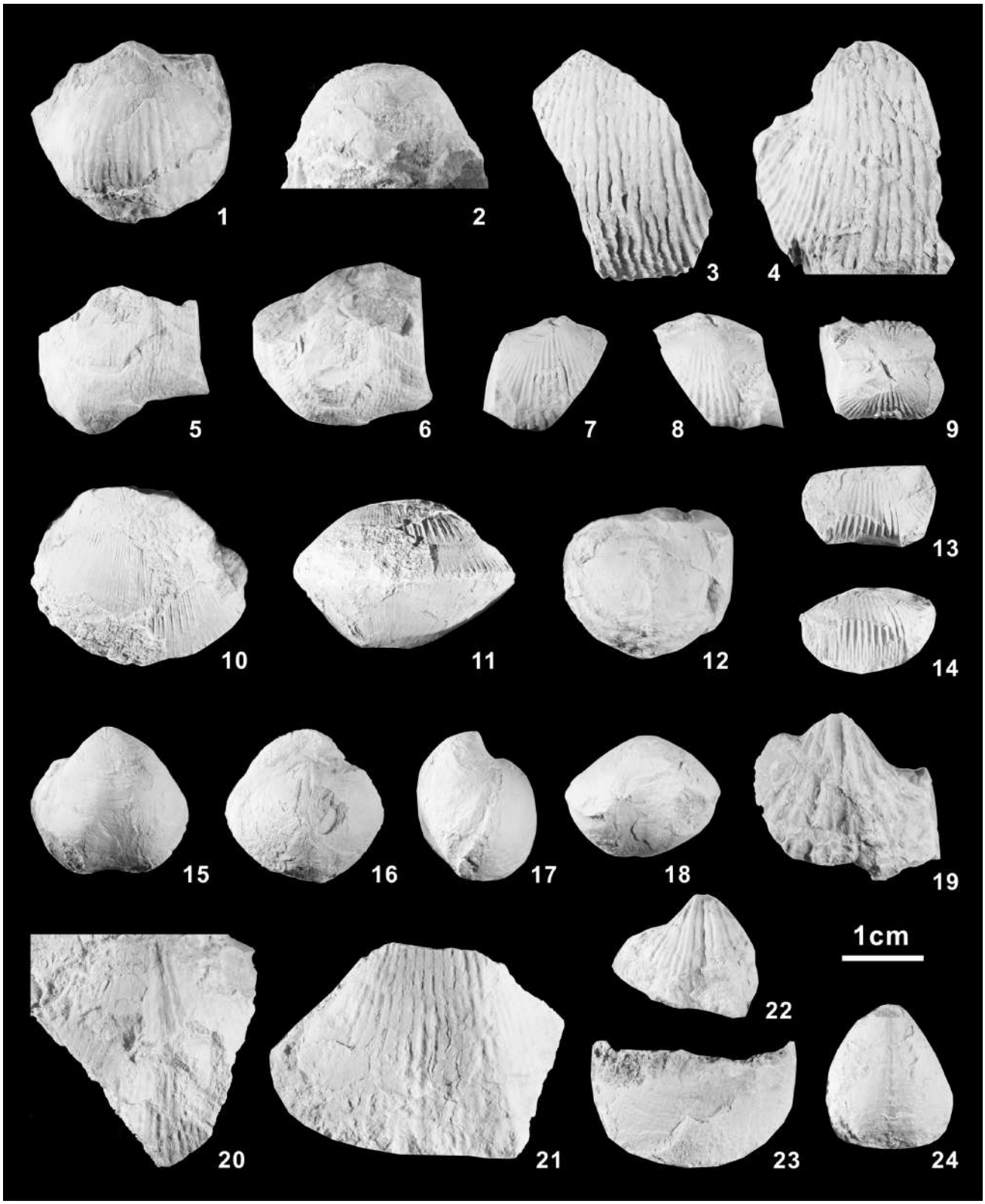

Figure 15. Brachiopod fossils from the Fengshan section (SABS). 1, 2, **Haydenella kiangsiensis** ***(Kayser, 1883). ventral and posterior views, 68.3 m. 3, 4,*** **Tyloplecta yangtzeensis** ***(Frech, 1911). 3, 4, ventral views, 68.3 m. 5, 6,*** **Transennatia gratiosa** ***(Waagen, 1884). ventral and posterior views, 15.5 m. 7-9,*** **Urushtenoidea crenulata** ***(Ting, 1962). ventral, dorsal and posterior views of a conjoined shell, 27 m. 10, 11,*** **Orthotichia** ***sp. dorsal and anterior views, 68.3 m. 12,*** **Enteletes kayseri** ***Waagen, 1883. lateral view, 32 m. 13, 14, Uncinunellina timorensis (Beyrich, 1864). ventral and anterior views, 20.7 m. 15-18,*** **Juxathyris guizhouensis** ***(Liao, 1980). ventral, dorsal, lateral and anterior views of a conjoined shell, 68.3 m. 19,*** **Zhejiangospirifer abnormalis** ***Liang, 1990. ventral view, 15.3 m. 20-22,*** **Alphaneospirifer anshunensis** ***(Liao, 1980), ventral view, 39 m; ventral view, 39 m; ventral view, 15.5 m. 23,*** **Permophricodothyris elegantula** ***(Waagen, 1883). ventral view of anterior portion of ventral valve, 17.8 m. 24,*** **Martinia** ***sp. ventral view, 23 m.***

was not detected in this study (Fig. 7). However, two values in the basal part of the section and nine values in the basal part of the Heshan Formation around 0.7070-0.7072 (blue points in Fig. 7) are very close to the Capitanian minimum.

To investigate the reasons producing the profound offset between the Fengshan section and global data is beyond the scope of the present paper. Many reasons such as the intensity of continental weathering, volcanism, diagenetic effects and different leaching methods may lead to variations in $^{87}Sr/^{86}Sr$. Since the average $^{87}Sr/^{86}Sr$ ratio at the Fengshan section is much higher than that of the Penglaitan section and many samples yield Mn/Sr > 1, global factors such as continental weathering, volcanism etc. can be excluded. Depositional water depth may be another reason to affect the results of $^{87}Sr/^{86}Sr$ ratio. However, facies analysis indicates that the GLB interval at the Fengshan and Penglaitan sections are both characterized by shallow shoal and bioherm settings (see below). Thus, it seems that diagenetic alternation of the samples at Fengshan is the most likely reason to produce higher $^{87}Sr/^{86}Sr$ ratios.

Magnetostratigraphy

Magnetic polarity zones can serve as a very useful tool for global correlation in both marine and terrestrial sequences. Magnetostratigraphic investigation was carried out by Manfred Menning and Shuzhong Shen in the Laibin area during 1994. They collected 640 oriented cylinders from the Chihsia, Maokou and basal part of the Heshan formations at the Tieqiao section and from the GLB interval at the Penglaitan section. Partial or total remagnetization complicates the magnetostratigraphic research (Menning et al., 1996) and so far no result has been published. More than 150 paleomagnetic samples were collected from the new Penglaitan section. Unfortunately, a preliminary test suggests that most of those samples suffered subsequent remagnetization. To establish a magnetostratigraphical framework, high-resolution samples across the GLB at the Fengshan section have been collected as well (Fig. 6E). A new high-resolution magnetostratigraphic sequence (ca. 260.85-258.75 Ma) on the Fengshan section in South China is established. Below the GLB, the magnetic polarity sequences are characterized by a mixed interval consisting of six normal (FS1n-FS6n) and six reverse (FS1r-FS6r) magnetozones. In the early Lopingian three magnetozones (FS7r, FS7n, and FS8r) are recognized. The GLB is in the reversed polarity interval (FS7r) (Zhang et al., in preparation). The *Jinogondolella granti* Zone is within the upper part of normal magnetozone FS6n and the reverse magnetozone FS7r, the *Clarkina postbitteri* Zone is within FS7r, which is 0.75 cm above the boundary between FS6n and FS7r. The *C. dukouensis* Zone is across three polarity zones from FS7r to FS8r.

Generally, the Carboniferous to early Guadalupian belongs to the reverse polarity Kiaman Superchron; whereas, the interval from the mid-Guadalupian and above belongs to Permian-Triassic mixed polarity Illawarra Superchron. Its boundary is marked by the first normal polarity zone called Illawarra Reversal largely in the Wordian (Hounslow and Balabanov, 2018). The Capitanian is normal polarity dominated (Jin et al., 2000; Steiner, 2006; Hounslow and Balabanov, 2018), but detailed polarity zones and their biostratigraphic and geochronologic constraints are unclear so far. The Fengshan section, for the first time, provided a high-resolution magnetostratigraphical timescale and will have great potential for correlation across the GLB between the marine and terrestrial sequences (Zhang et al., in preparation).

Recently, high-resolution samples for magnetostratigraphy at the new Penglaitan GSSP section were collected and analyzed. A reversed magnetozone from the top of the conodont *Clarkina granti* to the lower part of *C. dukounesis* Zone, which is correlative with FS7r at Fengshan, is defined. Unfortunately, partial remagnetization in the Middle Jurassic and Middle Triassic hampered establishing a high-resolution magnetostratigraphic sequence across the GLB at the Penglaitan GSSP section (Zhang et al., in preparation).

Lithofacies and Sequence Stratigraphy

The Fengshan section is composed of an 87 m-thick carbonate sequence with diverse and abundant fossils (Figs. 7, 16). The lowest 5.3 m (Unit 0) consists mainly of dark grey, thin- to medium-bedded packstone, wackestone and lime mudstone. The upper part is rich in chert nodules, and the lower part contains abundant thin- to medium-bedded chert. Fossils in limestones are dominated by sponge spicules and minor calcispheres. Bioclasts in chert nodules and bedded cherts are dominated by benthic fossils, such as crinoids and gastropods. The lithofacies and biofacies indicate that Unit 0 was deposited in a deep shelf environment below the storm-wave base, representing the final highstand stage before the global end-Guadalupian regression.

Overlying the basal deep-shelf facies is a set of light grey, medium- to thick-bedded bioclastic grainstone (Units 1 to 20) (Fig. 16A), intercalated by packstone, wackestone, and rudstone. Fossils in this interval are dominated by abraded debris of shallow benthos, such as crinoids, brachiopods, gastropods, foraminifers, bryozoans, calcareous sponges, and *Tubiphytes*. At the base of this interval, the sedimentary environment changed from the deep shelf settings to shallow shoal settings, marking a rapid shallowing representing the onset of the great end-Guadalupian regression event. Therefore, this surface corresponds to a significant drop of relative sea level and represents a type 1 sequence boundary.

Units 21 and 22 comprise mainly light grey or dark reddish grey, thick- to very thick-bedded sponge bafflestone (Fig. 16B), and minor rudstone. Calcareous sponges, mainly sphinctozoan and inozoan sponges, dominate the baffling fauna. The spaces between baffling sponges are filled mainly by lime muds, with minor calcite-spar-filling voids. Some gastropods and crinoid debris are present sporadically in the lime mud. The lithofacies and biofacies demonstrated that this interval represents low- to moderate-energy reef facies formed below the fair-weather wave base (FWB), representing a minor higher-order transgression during the long-term end-Guadalupian lowstand stage of the relative sea level.

The reef limestone of Unit 22 is overlain by a thick succession (29.9 m) of light grey to greyish white, thick- to very thick-bedded, bioclastic packstone, grainstone, and rudstone (Unit 23) (Fig. 16C), with a 1.9 m-thick sponge bafflestone on the top (Unit 24) (Fig. 16D). Fossils are dominated by crinoid skeletons, small foraminifers, fusulines, and brachiopods, bryozoans, and calcareous sponges. Similar to the interval of Units 1 to 20, Units 23 and 24 represent mainly the high-energy, agitated bioclastic shoal or open marine platform facies above the FWB (Unit 23) with a minor transgression in the topmost part (Unit 24).

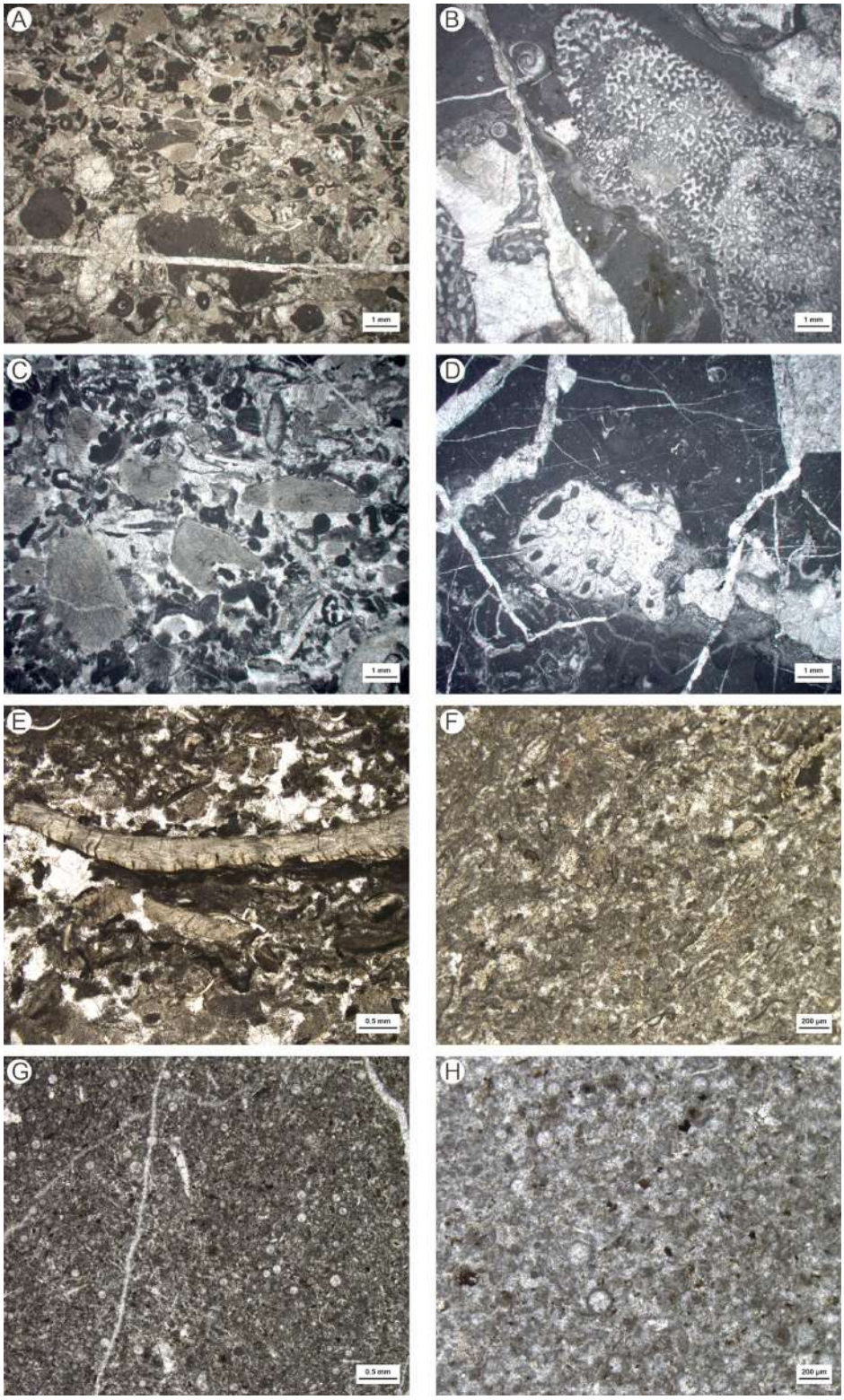

Figure 16. Sedimentary microfacies of the Maokou and Heshan formations of the Fengshan section (SABS). A, shoal facies, bioclastic grainstone containing abundant crinoid debris and* Tubiphytes*, Unit 3 (4.75 m). B, reef facies, sponge bafflestone showing the dominance of calcareous sponge and minor gastropods in lime mud matrices, Unit 22 (21.5 m). C, shoal facies, crinoid-bioclast grainstone consisting of abundant crinoid debris, foraminifers, and micritic bioclasts, Unit 23 (50.6 m). D, reef facies, sponge bafflestone showing the calcareous sponge-dominant fossil group and the lime mud-rich matrix, Unit 24 (57.7 m). E, subtidal zone facies. bioclastic grainstone consisting mainly of abraded debris of crinoids, ostracods, and brachiopods, Unit 26 (61.2 m). F, subtidal zone facies, bioclastic packstone containing abraded debris of crinoids, ostracods, small foraminifers, and micritic bioclasts, Unit 26 (62 m). G, deep shelf facies, fecal pellet-calcisphere wackestone showing common calcispheres and worn fecal pellets, as well as some ostracods, Unit 28 (64 m). H, deep shelf facies. Calcisphere-bioclast packstone composed mainly of calcispheres and micritic fossil debris, Unit 29 (65.3 m).

The topmost 3 m of the Maokou Formation is composed of light grey to dark grey, thin- to medium-bedded or nodular, bioclastic grainstone/packstone/wackestone (Fig. 16E, F). Grains are dominated by heavily abraded skeletons of crinoids, brachiopods, ostracods, and foraminifers. Greyish-green clay minerals altered from volcanic ash are common in this interval. The lithofacies and biofacies suggest that this interval formed in a high- to moderate-energy subtidal zone above the FWB, representing the shallowest part of the topmost Maokou Formation. This interval corresponds to the uppermost lowstand system tract during the end-Guadalupian regression which co-occurs with Emeishan volcanism in South China.

The basal Heshan Formation comprises dark grey to greyish black, thin- to medium-bedded wackestone and lime mudstone with packstone interbeds (Fig. 16G, H). Fossils are dominated by calcispheres, sponge spicules, and minor thin-shelled bivalves, ostracods, echinoderms, and fecal pellets. All these features indicate that this interval was deposited in a deep shelf environment below the storm-wave base, representing a rapid transgression after the global end-Guadalupian regression.

Correlation Between the GSSP Section and SABS

The Fengshan SABS section is basically consistent with the GSSP section at Penglaitan in terms of conodont and fusuline biostratigraphy and sedimentary sequence around the GLB interval (Figs. 7, 9). Thus, it is an ideal SABS to support the base-Lopingian GSSP. Future studies around GLB may rely on the Fengshan section because it has a long well-exposed succession and will not be flooded.

The conodont succession around the GLB including the *Jinogondolella prexuanhanensis*, *J. xuanhanensis*, *J. granti*, *Clarkina postbitteri* (including *C. postbitteri hongshuiensis*, *C. postbitteri postbitteri* and transitional morphotypes), *C. dukouensis*, *C. asymmetrica* and *C. guangyuanensis* zones in ascending order is fully recovered at the Fengshan section. Thus, they are completely correlative with those at the Penglaitan and Tieqiao sections in the Laibin area (Figs. 7, 9).

Fusulines dominated by *Lantschichites minima* and some small *Codonofusiella* in the uppermost part of the Maokou Formation are also comparable with those at Penglaitan and Tieqiao sections. In the Tieqiao section similar assemblages have been found in the topmost part of Maokou Formation which include *Metadoliolina douvillei, M. spheroidea, Lepidolina parasuschanica, Schwagerina pseudocompacta*, *Chusenella zhonghuaensis, Kahlerina sinensis, Lantschichites minima* and *Reichelina changanchiaoensis*. *Yabeina* and *Lepidolina* have not been found at the Fengshan section. In the Tieqiao section, the third fusuline assemblages contain both *Yabeina gubleri* and *Metadoliolina douvillei* (Shen et al., 2007). A slight difference is that the basal part of the Heshan Formation at Penglaitan and Tieqiao is characterized by the *Codonofusiella kueichowensis* Zone, but representative elements of this zone have not been found at the Fengshan section. *Codonofusiella* species are abundant in the topmost part of the Guadalupian and *Reichelina changhsingensis* ranges across the GLB at the Fengshan section. In addition, *Lantschichites minima* ranges into the basal part of the Wuchiapingian at Penglaitan (Wang et al., 2020), but it is restricted to the Maokou Formation at Fengshan.

Lithologically, the thick-bedded Laibin Limestone in the topmost part of the Maokou Formation at Penglaitan and Tieqiao in the Laibin area, which represents a lowstand system tract deposited continuously on the slope setting in the GLB interval, is also well developed at the Fengshan section. A minor difference is that the equivalent massive Laibin Limestone at Fengshan contains relatively less crinoid fragments and more abundant fusulines and foraminifers, and it is characterized by the sponge-bryozoan-algae bioherm facies. The topmost part of the Laibin Limestone at Penglaitan contains greenish tuffaceous ashes in the coarse crinoid bioclastic limestone (Fig. 9A), which directly indicates a temporal link with the Emeishan large igneous province in southwest China. These ashes have been also observed at the Fengshan section (Fig. 9B).

Furthermore, high-resolution magnetic polarity zones are established at the Fengshan section. This magnetostratigraphy will provide a basis for the correlation between marine and terrestrial sequences around the GLB. $\delta^{13}C_{carb}$ values across the GLB at the Penglaitan show a gradual increase from 3.7‰ in the base of *Jinogondolella granti* Zone to 5.06‰ in the basal part of *Clarkina postbitteri* Zone, followed by a decline of ~ 2‰ in the upper part of *C. dukouensis*. The broad interval with relatively low values in the *Jinogondolella xuanhanensis* Zone and the generally increasing $\delta^{13}C_{carb}$ trends in the uppermost part of the *J. xuanhanensis* Zone are largely comparable between the Penglaitan and Fengshan sections (Fig. 9) (Shen et al., 2020). However, obvious differences are also present. The Penglaitan section has higher $\delta^{13}C_{carb}$ values and does not have multiple excursions across the GLB. All the $\delta^{13}C_{carb}$ chemostratigraphical signals need to be investigated if they suffered diagenesis because previous reports of those $\delta^{13}C_{carb}$ excursions are in different horizons and quite variable in magnitude and time (Isozaki et al., 2007; Wignall et al., 2009; Bond et al., 2010; Chen et al., 2011; Nishikane et al., 2011; Liu et al., 2013; Shen et al., 2013).

In summary, the base-Wuchiapingian is defined by the FAD of the conodont *Clarkina postbitteri* within the lineage from *Jinogondolella granti*→*Clarkina postbitteri*→*C. dukouensis*. The secondary markers for the base of the Wuchiapingian Stage include a geochronologic age 259.51 ± 0.21 Ma and potential more precise ID-TIMS dates from the GSSP section, a distinct global regression at the GLB, the disappearance of large fusulines slightly below the GLB, the reversal porality zone FS7r and potential $\delta^{13}C_{carb}$ isotope excursions with global significance around the GLB.

Correlation with Other Regions

Other Areas in South China

The conodont succession established from the Fengshan, Penglaitan and Tieqiao sections can be mostly recognized in many other sections in South China. However, the *Jinogondolella granti* and *Clarkina postbitteri* zones in the GLB interval are largely unidentifiable and represented by a distinct unconformity indicated by the Wangpo Shale, a purple limonite bed and greenish volcanic ash with no conodonts (Mei and Wardlaw, 1996; Yuan et al., 2017, 2019; Hou et al., 2020). The underlying *Jinogondolella xuanhanensis* Zone and the overlying *Clarkina dukouensis* Zone can be widely identified in most areas of South China, suggesting sea water withdrawal in South China in the latest

Jinogondolella xuanhanensis Zone and returned in the *Clarkina dukouensis* Zone although at different times in different sections (Hou et al., 2020).

Sun and Xia (2006) recognized some *Clarkina postbitteri hongshuiensis* in the Dachongling section in Pingxiang, Guangxi. However, they are difficult to identify because the figured specimens are broken and unclear. Zhang et al. (2008) recognized the *C. postbitteri postbitteri* Subzone in the Maoershan section, Hubei, South China. However, most illustrated specimens appear to have serrations (e.g., Zhang et al., 2008, pl. 2, fig. 4), which is a character of *Jinogondolella*. Other specimens may be assignable to *Clarkina leveni* (e.g., Zhang et al., 2008, pl. 3, fig. 10). Shen and Zhang (2008) recognized this zone in the uppermost part of the Douling Formation in Chenzhou, Hunan. Thus, this zone has only been recognized in a few localities of South China.

North America

The Guadalupian Series and its three component stages are represented by the sequence in the Guadalupe and Glass Mountains areas and it is overlain by the evaporite deposits of the Castile Formation in North America. Most of the conodont zones of the Capitanian Stage including the *Jinogondolella postserrata*, *J. shannoni*, *J. altudaensis*, *J. prexuanhanensis* and *J. xuanhanensis* zones can be recognized in both South China and North America, providing a good correlation basis for the Capitanian Stage between South China and North America (Mei et al., 1994a; Wardlaw et al., 1999; Shen et al., 2020). However, the conodont zones above the *J. prexuanhanensis* zone are controversial between North America and South China (Mei et al., 1998; Wang, 2000, 2001; Henderson et al., 2002; Kozur and Wang, 2002; Lambert et al., 2002) and they all show some disagreement over the FAD of *Clarkina postbitteri*, its identification and evolutionary lineage. Rare specimens of *Jinogondolella granti* and *Clarkina postbitteri hongshuiensis* were reported from the Reef Trail Member of the Bell Canyon Formation in the Guadalupe Mountains National Park in West Texas (Lambert et al., 2002;Lambert et al., 2010; Wardlaw and Nestell, 2010; Bell et al., 2015). Based on the latest study on the Guadalupian conodonts from West Texas and South China, these specimens were re-assigned to *Jinogondolella altudaensis*, which is the most common species in this member (Yuan et al., 2017; Shen et al., 2020). Wardlaw and Nestell (2010) illustrated two specimens as *Clarkina postbitteri hongshuiensis* from the Apache Mountains, West Texas. They coexist with very abundant *Jinogondolella altudaensis* in the same samples. These two specimens still have a broad platform, dense denticles, and a very small cusp, which are the characters typical within the sample population of *J. altudaensis*. Thus, Yuan et al. (2017) did not regard them as *Clarkina postbitteri hongshuiensis* and re-assigned these two specimens to *Jinogondolella altudaensis* based on a sample population approach. The strata above the *J. altudaensis* at the Apache Mountains are represented by the evaporite deposits of the Castile Formation (Yuan et al., 2017; Shen et al., 2020). According to Yuan et al. (2017), the topmost zone in West Texas is near the *Jinogondolella prexuanhanensis* Zone, and no transitional population from *J. altudaensis* to *Clarkina postbitteri hongshuiensis* has been found and there are at least three more conodont zones (the *Jinogondolella prexuanhanensis*, *J. xuanhanensis* and *J. granti* zones) between the *J. altudaensis* Zone and the *Clarkina postbitteri* Zone in South China. Therefore, the evolutionary relationship between *Jinogondolella altudaensis* and *Clarkina postbitteri hongshuiensis* cannot be demonstrated based on the West Texas specimens.

Problems for the GLB correlation between South China and North America were also raised by ammonoids (Zhou, 2017). Six Permian ammonoid zones were recognized in South China and the upper three zones are correlative with those from the Permian of Las Delicias, Coahuila, Mexico and west Texas, USA (Zhou, 2017), of which the uppermost *Eoaraxoceras spinosai-Difuntites furnishi* Zone from the 3rd Member of the Shaiwa Formation in Ziyun, Guizhou Province has been regarded as the counterpart of the *Eoaraxoceras spinosai-Difuntites* Zone of the upper Capitanian in Coahuila, Mexico and west Texas, USA (Miller, 1944; Wardlaw, 2000). Thus, ammonoids provide direct correlation between the uppermost Capitanian and the lower part of the 3rd Member of the Shaiwa Formation in Guizhou, South China (Zhou, 2017, fig. 9). However, Zhou (2017) assigned the *Eoaraxoceras spinosai-Difuntites furnishi* Zone in the 3rd Member of the Shaiwa Formation to the Wuchiapingian of South China because this zone is found between the 4th Member of the Shaiwa Formation containing the conodonts *Clarkina* cf. *guangyuanensis* and *C. subcarinata*, and the *Waagenoceras* Zone in the Chongtou Member below, which contains *Jinogondolella aserrata* and *J. postserrata* (Hao et al., 1999; Wang et al., 2016). Thus, Zhou (2017) claimed that the Wuchiapingian Stage in South China partly overlaps with the uppermost Guadalupian in Coahuila, Mexico and west Texas, USA. However, a re-examination suggests that none of the conodonts illustrated by Hao et al. (1999) from the 4th Member have been correctly identified. The single specimen assigned to "*Clarkina subcarinata*" only has a lower view, which is not identifiable. Even if those conodonts were of Wuchiapingian or Changhsingian in age, it does not indicate that the underlying 3rd Member is of Lopingian in age. On the contrary, the same latest Guadalupian ammonoid zone between the 3rd Member of the Shaiwa Formation and the uppermost Capitanian in Coahuila, Mexico and west Texas, USA suggests that the 3rd Member of the Shaiwa Formation is latest Capitanian in age. This correlation is supported by a subsequent conodont study in which *Sweetognathus inornatus* and *Sw. paraguizhouensis* (both may be assignable to the Guadalupian *Sw. subsymmetricus*) were reported from the 3rd Member of the Shaiwa Formation (Ji et al., 2009) in Ziyun, Guizhou, South China (Shen et al., 2019).

Chemostratigraphy across the GLB interval has been previously intensively studied in order to unravel the causes of the end-Guadalupian biotic crisis and environmental changes (Isozaki et al., 2007; Wignall et al., 2009; Bond et al., 2010; Saitoh et al., 2013; Shen et al., 2013). The different chemostratigraphical signals may have some potential to be used for the correlation around the GLB. However, so far many data are controversial due to different reasons.

Iran

The Permian and Lower Triassic succession in central Iran was first classified into 12 units, among which Units 1-7 belong to the Permian and Units 8-12 to the Lower and Middle Triassic. Units 1-3 were assigned to Surmaq Formation, which is largely lower and middle Guadalupian. The overlying Abadeh Formation consists of Units 4a, 4b and 5 of mainly black shale and thin-bedded limestone (Iranian-

Japanese-Research-Group, 1981; Taraz et al., 1981). Traditionally, the GLB in the Abadeh area was placed at the base of Unit 6, that is, the base of the Hambast Formation, marked by the brachiopod *Araxilevis* Bed followed by the ammonoid *Araxoceras tectum* Zone and the conodont *Clarkina leveni* Zone. A distinct lithologic boundary between Units 5 and 6 is well recognized in the outcrop at Abadeh, central Iran. The small and specialized fusuline *Codonofusiella* is abundant in Unit 5. A re-examination of the conodonts collected by Walter Sweet suggests that the base of the Hambast Formation contains the conodont *Clarkina dukouensis* and possibly *C. postbitteri* in the basal part of Unit 6 (Shen and Mei, 2010). Subsequent collecting of the conodont and geochemical samples suggests that the upper part of Unit 5 already contains *Clarkina* and some minor, but distinct $\delta^{13}C_{carb}$ fluctuations are present in the upper part of Unit 5 in association with the beginning of the rising trend of $^{87}Sr/^{86}Sr$ ratio (Liu et al., 2013). This GLB is also well recognized at the base of the Julfa Beds in the Kuh-e-Ali Bashi area of northwest Iran (Shen and Mei, 2010).

Oman

Middle Permian to Lower Triassic rocks are exposed at Buday'ah in the Oman Mountains, Oman. The Buday'ah Formation ranges from the Guadalupian to Lower Triassic. The GLB interval is developed in the basal part of the section. Unit 1 consists of pillow basalt that provided a base for the Permian-Triassic sedimentary succession above. These volcanic and sedimentary rocks formed in a deep oceanic setting along the southern margin of the Neotethys. Unit 2 is a dm-1.2 m thick pelagic red ammonoid-bearing limestone, which is overlain by the radiolarian-bearing cherts. The Wordian-Capitanian ammonoid *Timorites* sp. and *Waagenoceras* cf. *mojsisovicsiis* were reported in the basal part of this unit. In the topmost part of this unit, *Clarkina postbitteri hongshuiensis* was found and illustrated (Baud et al., 2012). A reexamination shows that the population is slightly different from those specimens at Penglaitan, but the horizon is very close to the GLB based on the overlying Wuchiapingian radiolarians *Pseudoalbaillella fusiformis* and *Follicucullus ventricosus*.

Accessibility and Protection

The new Penglaitan GSSP section is about 10 m above the original GSSP section and is still flooded periodically during the high water season of the Hongshui River. The SABS at Fengshan is located in a small valley in a low mountain area near Fengshan Town with direct paved road access. A simple highway is available directly to the section. The section is easily accessible by any vehicle, and it will be fully protected by the local government after it is ratified as the SABS. Heavy vegetation on either side of the creek will be cleared. In addition, a dedicated access road will be built along the section, and a monument will be erected. Sample collecting for research purposes will be guaranteed.

Acknowledgements

This work is supported by the National Natural Science Foundation of China (42293280, 42272031, 42250104, 42261144668) and Strategic Priority Research Program (B) of the Chinese Academy of Sciences (XDB26000000).

References

Angiolini, L., and Carabelli, L., 2010, Upper Permian brachiopods from the Nesen formation, North Iran. Special Papaer in Palaeontology, n. 84, pp. 41–90.

Baud, A., Richoz, S., Beauchamp, B., Cordey, F., Grasby, S., Henderson, C. M., Krystyn, L., and Nicora, A., 2012, The Buday'ah Formation, Sultanate of Oman: A Middle Permian to Early Triassic oceanic record of the Neotethys and the late Induan microsphere bloom. Journal of Asian Earth Sciences, v. 43, pp. 130–144.

Bell, G.L.J., Hearst, J.M., Nestell, M.K., Nestell, G.P., and Lambert, L.L., 2015, Stratigraphic framework and biostratigraphic significance of the terminal Guadalupian Reef Trail Member, Bell Canyon Formation in the Patterson Hills, Type Guadalupian Area, Texas. Stratigraphy, v. 12, pp. 93–107.

Bellefroid, E.J., Planavsky, N.J., Miller, N.R., Brand, U., and Wang, C., 2018, Case studies on the utility of sequential carbonate leaching for radiogenic strontium isotope analysis. Chemical Geology, v. 497, pp. 88–99.

Bond, D.P.G., Hilton, J., Wignall, P.B., Ali, J.R., Stevens, L.G., Sun, Y.D., and Lai, X.L., 2010, The Middle Permian (Capitanian) mass extinction on land and in the oceans. Earth-Science Reviews, v. 102, pp. 100–116.

Chen, B., Joachimski, M.M., Sun, Y.D., Shen, S.Z., and Lai, X.L., 2011, Carbon and conodont apatite oxygen isotope records of Guadalupian–Lopingian boundary sections: Climatic or sea-level signal?. Palaeogeography, Palaeoclimatology, Palaeoecology, v. 311, pp. 145–153.

Chen, J., and Xu, Y.G., 2019, Establishing the link between Permian volcanism and biodiversity changes: Insights from geochemical proxies. Gondwana Research, v. 75, pp. 68–96.

Clapham, M.E., Shen, S.Z., and Bottjer, D.J., 2009, The double mass extinction revisited: reassessing the severity, selectivity, and causes of the end-Guadalupian biotic crisis (Late Permian). Paleobiology, v. 35, pp. 32–50.

Crippa, G., and Angiolini, L., 2012, Guadalupian (Permian) brachiopods from the Ruteh Limestone, North Iran. Geoarabia, v. 17, pp. 125–176.

Erwin, D.H., 2006, Extinction: How life on Earth nearly ended 250 million years ago. Princeton University Press, New Jersey, 296 p.

Fan, J.X., Shen, S.Z., Erwin, D.H., Sadler, P.M., MacLeod, N., Cheng, Q.M., Hou, X.D., Yang, J., Wang, X.D., Wang, Y., Zhang, H., Chen, X., Li, G.X., Zhang, Y.C., Shi, Y.K., Yuan, D.X., Chen, Q., Zhang, L.N., Li, C., and Zhao, Y.Y., 2020, A high-resolution summary of Cambrian to Early Triassic marine invertebrate biodiversity. Science, v. 367, pp. 272–277.

Garbelli, C., Angiolini, L., Shen, S.Z., Crippa, G., Yuan, D.X., Bahrammanesh, M., Abbasi, S., and Birjandi, M., 2014, Additional brachiopod findings from the Lopingian succession of the Ali Bashi Mountains, NW Iran. Rivista Italiana di Paleontologia e Stratigrafia, v. 120, pp. 119–126.

Ghaderi, A., Garbelli, C., Angiolini, L., Ashouri, A.R., Korn, D., Rettori, R., and Gharaie, M.H.M., 2014, Faunal change near the end-Permian extinction: the brachiopods of the Ali Bashi Mountains, NW Iran. Rivista Italiana di Paleontologia e Stratigrafia, v. 120, pp. 27–59, 25pls.

Hao, W.C., Yao, J.X., and Liu, J.B., 1999, Permian conodonts from the Shaiwa section in Ziyun, Guizhou. In: Yao, A., Ezaki, Y., Hao, W.C., and Wang, X.P. (Eds.), Biotic and Geological Developments of the Paleo-Tethys in China, Beijing, Peking University Press, pp. 73–79.

Haq, B.U., and Schutter, S.R., 2008, A chronology of Paleozoic sea-level changes. Science, v. 322, pp. 64–68.

He, B., Xu, Y.G., Huang, X.L., Luo, Z.Y., Shi, Y.R., Yang, Q.J., and Yu,

S.Y., 2007, Age and duration of the Emeishan flood volcanism, SW China: Geochemistry and SHRIMP zircon U-Pb dating of silicic ignimbrites, post-volcanic Xuanwei Formation and clay tuff at the Chaotian section. Earth and Planetary Science Letters, v. 255, pp. 306–323.

Head, M.J., Aubry, M.P., Piller, W.E., and Walker, M., 2022, The Standard Auxiliary Boundary Stratotype: a proposed replacement for the Auxiliary Stratotype Point in supporting a Global boundary Stratotype Section and Point (GSSP). Episodes, in press.

Henderson, C.M., Mei, S.L., and Wardlaw, B.R., 2002, New conodont definitions at the Guadalupian-Lopingian boundary. Carboniferous and Permian of the world; XIV ICCP proceedings: Memoir Canadian Society of Petroleum Geologists, v. 19, pp. 725–735.

Hou, Z.S., Fan, J.X., Henderson, C.M., Yuan, D.X., Shen, B.H., Wu, J., Wang, Y., Zheng, Q.F., Zhang, Y.C., Wu, Q., and Shen, S.Z., 2020, Dynamic palaeogeographic reconstructions of the Wuchiapingian Stage (Lopingian, Late Permian) for the South China Block. Palaeogeography, Palaeoclimatology, Palaeoecology, v. 546, pp. 109667.

Hounslow, M.W., and Balabanov, Y.P., 2018, A geomagnetic polarity timescale for the Permian, calibrated to stage boundaries. Geological Society, London, Special Publications, v. 450, pp. 61–103.

Hu, S.Z., 1994, On the event of Dongwu Movement and its relation with Permian subdivision. Journal of Stratigraphy, v. 18, pp. 309–315.

Huang, H., Huyskens, M.H., Yin, Q.Z., Cawood, P.A., Hou, M.C., Yang, J.H., Xiong, F.H., Du, Y.S., and Yang, C.C., 2022, Eruptive tempo of Emeishan large igneous province, southwestern China and northern Vietnam: Relations to biotic crises and paleoclimate changes around the Guadalupian-Lopingian boundary. Geology, v. 50, pp. 1083–1087.

Iranian-Japanese-Research-Group, 1981, The Permian and Lower Triassic Systems in Abadeh region, central Iran. Memoirs of the Faculty of Sciences, Kyoto University, Series of Geology and Mineralogy, v. 47, pp. 61–133, pls. 131–136.

Isozaki, Y., Kawahata, H., and Ota, A., 2007, A unique carbon isotope record across the Guadalupian–Lopingian (Middle–Upper Permian) boundary in mid-oceanic paleo-atoll carbonates: The high-productivity "Kamura event" and its collapse in Panthalassa. Global and Planetary Change, v. 55, pp. 21–38.

Ji, X.X., Li, M., and Feng, H Z., 2009, Middle Permian conodonts from the Shaiwa Group in Sidazhai area, Ziyun County, Guizhou. Geological Review, v. 55, pp. 113–120.

Jin, Y.G., 1993, Pre-Lopingian benthos crisis. Comptes Rendus XII ICC-P, Volume 2: Buenos Aires, pp. 269–278.

Jin, Y.G., 2000, Conodont definition on the basal boundary of Lopingian stages: A report from the International Working Group on the Lopingian Series. Permophiles, v. 36, pp. 37–40.

Jin, Y.G., Zhang, J., and Shang, Q.H., 1994, Two phases of the end-Permian mass extinction. In: Embry, A.F., Beauchamp, B., and Glass, D.J. (Eds.), Canadian Society of Petroleum Geologists, Memoir 17, Volume 17: Calgary, Canadian Society of Petroleum Geologists, pp. 813–822.

Jin, Y.G., Shang, Q.H., and Cao, C.Q., 2000, Late Permian magnetostratigraphy and its global correlation. Chinese Science Bulletin, v. 45, pp. 698–705.

Jin, Y.G., Henderson, C.M., Wardlaw, B.R., and Glenister, B.F., 2001a, A commentary on the proposal for the GSSP for the Guadalupian/Lopingian boundary. Permophiles, v. 38, pp. 30–35.

Jin, Y.G., Henderson, C.M., Wardlaw, B.R., Glenister, B.F., Mei, S.L., Shen, S.Z., and Wang, X.D., 2001b, Proposal for the global stratotype section and point (GSSP) for the Guadalupian-Lopingian boundary. Permophiles, v. 39, pp. 32–42.

Jin, Y.G., Shen, S.Z., Henderson, C.M., Wang, X.D., Wang, W., Wang, Y., Cao, C.Q., and Shang, Q.H., 2006, The Global Stratotype Section and Point (GSSP) for the boundary between the Capitanian and Wuchiapingian stage (Permian). Episodes, v. 29, pp. 253–262.

Kani, T., Hisanabe, C., and Isozaki, Y., 2013, The Capitanian (Permian) minimum of $^{87}Sr/^{86}Sr$ ratio in the mid-Panthalassan paleo-atoll carbonates and its demise by the deglaciation and continental doming. Gondwana Research, v. 24, pp. 212–221.

Kani, T., Isozaki, Y., Hayashi, R., Zakharov, Y., and Popov, A., 2018, Middle Permian (Capitanian) seawater 87Sr/86Sr minimum coincided with disappearance of tropical biota and reef collapse in NE Japan and Primorye (Far East Russia). Palaeogeography, Palaeoclimatology, Palaeoecology, v. 499, pp. 13–21.

Kani, T., and Isozaki, Y., 2021, The Capitanian Minimum: A Unique Sr Isotope Beacon of the Latest Paleozoic Seawater. Frontiers in Earth Science, v. 9, pp. 662581.

Korte, C., and Ullmann, C.V., 2016, Permian strontium isotope stratigraphy. In: Lucas, S.G., and Shen, S.Z. (Eds.), The Permian Timescale, The Geological Society of London, London, v. 450, pp. 105–118.

Korte, C., Jasper, T., Kozur, H.W., and Veizer, J., 2006, Sr^{87}/Sr^{86} record of Permian seawater. Palaeogeography Palaeoclimatology Palaeoecology, v. 240, pp. 89–107.

Kotljar, G.V., Zakharov, Y.D., Koczyrkevicz, B.V., Kropatcheva, G.S., Rostovcev, K.O., Chedija, I.O., Vuks, G.P., and Guseva, E.A., 1983, Pozdnepermskii Etap Evoliutsii Organicheskogo Mira, Dzhul'finskii i Dorashamskii Iarusy SSSR (Evolution of the latest Permian biota, Dzhulfian and Dorashamian regional stages in the USSR). Leningrad, Nauka, 200 p.

Kozur, H.W., and Wang, C.Y., 2002, Comments to the base of the Lopingian Series defined in the Penglaitan section. Permophiles, v. 40, pp. 25–30.

Lambert, L.L., Wardlaw, B.R., Nestell, M.K., and Nestell, G.P., 2002, Latest Guadalupian (Middle Permian) conodonts and foraminifers from West Texas. Micropaleontology v. 48, pp. 343–364.

Lambert, L.L., Bell, G.L., Fronimos, J.A., Wardlaw, B.R., and Yisa, M.O., 2010, Conodont biostratigraphy of a more complete Reef Trail Member section near the type section, latest Guadalupian Series type region. Micropaleontology, v. 56, pp. 233–253.

Li, Q., Yang, S., Azmy, K., Chen, H.D., Hou, M.C., Wang, Z.J., Xu, S.L., Yang, D., Zhang, X.H., and Chen, A.Q., 2021, Strontium isotope evolution of Middle Permian seawater in the Sichuan Basin, South China: Possible causes and implications. Palaeogeography, Palaeoclimatology, Palaeoecology, v. 565, pp. 110188.

Li, Y.J., He, H.Y., Ivanov, A.V., Demonterova, E.I., Pan, Y.X., Deng, C.L., Zheng, D.W., and Zhu, R.X., 2018, $^{40}Ar/^{39}Ar$ age of the onset of high-Ti phase of the Emeishan volcanism strengthens the link with the end-Guadalupian mass extinction. International Geology Review, v. 60, pp. 1906–1917.

Liu, X.C., Wang, W., Shen, S.Z., Gorgij, M.N., Ye, F.C., Zhang, Y.C., Furuyama, S., Kano, A., and Chen, X.Z., 2013a, Late Guadalupian to Lopingian (Permian) carbon and strontium isotopic chemostratigraphy in the Abadeh section, central Iran. Gondwana Research, v. 24, pp. 222–232.

McArthur, J.M., Howarth, R.J., and Shields, G.A., 2012, Strotium isotope stratigraphy. In: Gradstein, F.M., Ogg, J.G., Schmitz, M.D., and Ogg, G.M. (Eds.), The Geological time scale 2012, Volume vol. 2, Elsevier, Amsterdam, pp. 127–144.

McArthur, J.M., Howarth, R.J., Shields, G.A., and Zhou, Y., 2020, Strontium isotope stratigraphy. In: Gradstein, F.M., Ogg, J.G., Schmitz, M.D., and Ogg, G.M. (Eds.), Geologic Time Scale 2020, Volume 1, Elsevier, Amsterdam, pp. 211–238.

Mei, S.L., and Wardlaw, B.R., 1996, On the Permian "*Liangshanensis-bitteri*" zone and the related problems In: Wang, H.Z., and Wang, X.L. (Eds.), Centennial Memorial Volume of Professor Sun Yunzhu: Stratigraphy and Palaeontology, China University of Geosciences Press, Wuhan, pp. 130–140.

Mei, S.L., and Henderson, C.M., 2001, Evolution of Permian conodont provincialism and its significance in global correlation and paleoclimate implication. Palaeogeography, Palaeoclimatology, Palaeoecology, v. 170, pp. 237–260.

Mei, S.L., Jin, Y.G., and Wardlaw, B.R., 1994a, Succession of conodont

zones from the Permian "Kuhfeng" Formation, Xuanhan, Sichuan and its implications in global correlation. Acta Palaeontologica Sinica, v. 33, pp. 1–23.

Mei, S.L., Jin, Y.G., and Wardlaw, B.R., 1994b, Zonation of conodonts from the Maokouan-Wuchiapingian boundary strata, South China. In: Jin, Y.G., Utting, J., and Wardlaw, B.R. (Eds.), Permian stratigraphy, environments and resources, Nanjing University Press, Nanjing, Palaeoworld, v. 4, pp. 225–233.

Mei, S.L., Jin, Y.G., and Wardlaw, B.R., 1998, Conodont succession of the Guadalupian-Lopingian boundary strata in Laibin of Guangxi, China and West Texas, USA. In: Jin, Y.G., Wardlaw, B.R., and Wang, Y. (Eds.), Permian stratigraphy, environments and resources, Nanjing University Press, Nanjing, Palaeoworld, v. 9, pp. 53–76.

Mei, S.L., Shi, X.Y., Chen, X.F., Sun, K.Q., and Yan, J.X., 1999, Permian Cisuralian and Guadalupian sequence stratigraphy in south Guizhou and central Guangxi and its relation to conodont evolution. Earth Science-Journal of China University of Geosciences, v. 24, pp. 21–31.

Menning, M., Jin, Y.G., and Shen, S.Z., 1996, The Illawarra Reversal (265 Ma) in the marine Permian, Guangxi, South China. In: Proceedings Abstracts to 30th International Geological Congress, Beijing, Volume 2, p. 9.

Miller, A.K., 1944, Part IV Permian cephalopods. In: King, R.E., Dunbar, C.O.J., Cloud, P.E., and Miller, A.K. (Eds.), Geology and Paleontology of the Permian Area Northwest of Las Delicias, Southwestern Coahuila, Mexico. Geological Society of America Special Paper, v. 52, pp. 71–127.

Nishikane, Y., Kaiho, K., Takahashi, S., Henderson, C.M., Suzuki, N., and Kanno, M., 2011, The Guadalupian-Lopingian boundary (Permian) in a pelagic sequence from Panthalassa recognized by integrated conodont and radiolarian biostratigraphy, Marine Micropaleontology, v. 78, pp. 84–95.

Ramezani, J., and Bowring, S.A., 2018, Advances in numerical calibration of the Permian timescale based on radioisotopic geochronology. Geological Society, London, Special Publications, v. 450, pp. 51–60.

Saitoh, M., Isozaki, Y., Ueno, Y., Yoshida, N., Yao, J.X., and Ji, Z.S., 2013, Middle–Upper Permian carbon isotope stratigraphy at Chaotian, South China: Pre-extinction multiple upwelling of oxygen-depleted water onto continental shelf. Journal of Asian Earth Sciences, v. 67–68, pp. 51–62.

Shellnutt, J.G., Denyszyn, S.W., and Mundil, R., 2012, Precise age determination of mafic and felsic intrusive rocks from the Permian Emeishan large igneous province (SW China). Gondwana Research, v. 22, pp. 118–126.

Shellnutt, J.G., Pham, T.T., Denyszyn, S.W., Yeh, M.W., and Tran, T.A., 2020, Magmatic duration of the Emeishan large igneous province: Insight from northern Vietnam. Geology, v. 48, pp. 457–461.

Shen, S.Z., 2018, Global Permian brachiopod biostratigraphy: an overview. Geological Society, London, Special Publications, v. 450, pp. 289–320.

Shen, S.Z., and Zhang, Y.C., 2008, Earliest Wuchiapingian (Lopingian, late Permian) brachiopods in southern Hunan, South China: implications for the pre-Lopingian crisis and onset of Lopingian recovery/radiation. Journal of Paleontology, v. 82, pp. 924–937.

Shen, S.Z., and Shi, G.R., 2009, Latest Guadalupian brachiopods from the Guadalupian/Lopingian boundary GSSP section at Penglaitan in Laibin, Guangxi, South China and implications for the timing of the pre-Lopingian crisis. Palaeoworld, v. 18, pp. 152–161.

Shen, S.Z., Sun, D.L., and Shi, G.R., 2003, A biogeographic mixed late Guadalupian (late Middle Permian) brachiopod fauna from an exotic limestone block at Xiukang in Lhaze county, Tibet. Journal of Asian Earth Sciences, v. 21, pp. 1125–1137.

Shen, S.Z., Henderson, C.M., Bowring, S.A., Cao, C.Q., Wang, Y., Wang, W., Zhang, H., Zhang, Y.C., and Mu, L., 2010, High-resolution Lopingian (Late Permian) timescale of South China. Geological Journal, v. 45, pp. 122–134.

Shen, S.Z., and Mei, S.L., 2010, Lopingian (Late Permian) high-resolution conodont biostratigraphy in Iran with comparison to South China zonation. Geological Journal, v. 45, pp. 135–161.

Shen, S.Z., Wang, Y., Henderson, C.M., Cao, C.Q., and Wang, W., 2007, Biostratigraphy and lithofacies of the Permian System in the Laibin-Heshan area of Guangxi, South China. Palaeoworld, v. 16, pp. 120–139.

Shen, S.Z., Cao, C.Q., Zhang, H., Bowring, S.A., Henderson, C.M., Payne, J.L., Davydov, V.I., Chen, B., Yuan, D.X., Zhang, Y.C., Wang, W., and Zheng, Q.F., 2013, High-resolution $\delta^{13}C_{carb}$ chemostratigraphy from latest Guadalupian through earliest Triassic in South China and Iran. Earth and Planetary Science Letters, v. 375, pp. 156–165.

Shen, S.Z., Zhang, H., Zhang, Y.C., Yuan, D.X., Chen, B., He, W.H., Mu, L., Lin, W., Wang, W.Q., Chen, J., Wu, Q., Cao, C.Q., Wang, Y., and Wang, X.D., 2019, Permian integrative stratigraphy and timescale of China. Science in China Series D: Earth Sciences, v. 62, pp. 154–188.

Shen, S.Z., Yuan, D.X., Henderson, C.M., Wu, Q., Zhang, Y.C., Zhang, H., Mu, L., Ramezani, J., Wang, X.D., Lambert, L.L., Erwin, D.H., Hearst, J.M., Xiang, L., Chen, B., Fan, J.X., Wang, Y., Wang, W Q., Qi, Y.P., Chen, J., Qie, W.K., and Wang, T.T., 2020, Progress, problems and prospects: An overview of the Guadalupian Series of South China and North America. Earth-Science Reviews, v. 211, pp. 103412.

Sheng, J.Z., Jin, Y.G., 1994. Correlation of Permian deposits in China. Palaeoworld 4, 14–113.

Stanley, S.M., and Yang, X.N., 1994, A double mass extinction at the end of the Paleozoic Era. Science, v. 266, pp. 1340–1344.

Steiner, M.B., 2006, The magnetic polarity time scale across the Permian-Triassic boundary. In: Lucas, S.G., Cassinis, G., and Schneider, J.W. (Eds.), Non-marine Permian biostratigraphy and biochronology, The Geological Society, London, v. 265, pp. 15–38.

Sun, D.Y., and Xia, W.C., 2006, Identification of the Guadalupian-Lopingian boundary in the Permian in a bedded chert sequence, south China. Palaeogeography, Palaeoclimatology, Palaeoecology, v. 236, pp. 272–289.

Taraz, H., Golshani, F., Nakazawa, K., Shimizu, D., Bando, Y., Ishii, K., Murata, M., Okimura, Y., Sakagami, S., Nakamura, K., and Tokuoka, T., 1981, The Permian and the Lower Triassic Systems in Abadeh Region, Central Iran. Kyoto University, Faculty of Science (Geology and Mineralogy), Memoirs, v. 47, pp. 61–133.

Verna, V., Angiolini, L., Chaouachi, C., Soussi, M., Henderson, C.M., Davydov, V.I., Nicora, A., and Bougdar, M., 2010, Guadalupian brachiopods from Djebel Tebaga de Medenine, South Tunisia. Rivista Italiana di Paleontologia e Stratigrafia, v. 116, pp. 309–349.

Viaretti, M., Heward, A.P., Gementi, A., and Angiolini, L., 2022, Upper Cisuralian-lower Guadalupian brachiopods from the Qarari unit, Batain Plain, northeast Oman: Systematics, palaeoecology and correlation. Rivista Italiana di Paleontologia e Stratigrafia, v. 128, pp. 643–694.

Wang, C.Y., 2000, The base of the Lopingian Series-restudy of the Penglaitan section. Acta Micropalaeontologica Sinica, v. 17, pp. 1–17.

Wang, C.Y., 2001, Re-discussion of the base of the Lopingian Series. Permophiles, v. 38, pp. 27–29.

Wang, D.C., Jiang, H.S., Gu, S.Z., and Yan, J.X., 2016, Cisuralian–Guadalupian conodont sequence from the Shaiwa section, Ziyun, Guizhou, South China. Palaeogeography, Palaeoclimatology, Palaeoecology, v. 457, pp. 1–22.

Wang, W.Q., Garbelli, C., Zheng, Q.F., Chen, J., Liu, X.C., Wang, W., and Shen, S.Z., 2018, Permian $^{87}Sr/^{86}Sr$ chemostratigraphy from carbonate sequences in South China. Palaeogeography, Palaeoclimatology, Palaeoecology, v. 500, pp. 84–94.

Wang, W.Q., Katchinoff, J.A.R., Garbelli, C., Immenhauser, A., Zheng, Q.F., Zhang, Y.C., Yuan, D.X., Shi, Y.K., Wang, J.Y., Planavsky, N., and Shen, S.Z., 2021, Revisiting the Permian seawater $^{87}Sr/^{86}Sr$ record: New perspectives from brachiopod proxy data and stochastic oceanic box models. Earth-Science Reviews, v. 218, pp. 103679.

Wang, Y., Zhang, Y.C., Zheng, Q.F., Tian, X.S., Huang, X., and Luo, M., 2020, The early Wuchiapingian (late Permian) fusuline fauna from the Penglaitan Section, South China. Papers in Palaeontology, v. 6, pp.

485–499.
Wardlaw, B.R., 2000, Guadalupian conodont biostratigraphy of the Glass and Del Norte Mountains. In: Wardlaw, B.R., Grant, R.E., and Rohr, D.M. (Eds.), The Guadalupian Symposium, Smithsonian contributions to the Earth Sciences, Smithsonian Institution, Washington D.C., pp. 37–81.
Wardlaw, B.R., and Henderson, C.M., 2002, Reply to Kozur and Wang's Comments to the base of the Lopignian Series defined in the Penglaitan section. Permophiles, v. 40, pp. 31–32.
Wardlaw, B.R., and Nestell, M.K., 2010, Latest Middle Permian conodonts from the Apache Mountains, West Texas. Micropaleontology, v. 56, pp. 149–183.
Wardlaw, B.R., Lamberti, L.L., and Mei, S.L., 1999, Succession of latest Guadalupian (Permian) conodont faunas from South China and West Texas.In: Proceedings Proceedings of the International Conference on Pangea and the Paleozoic-Mesozoic transition, China University of Geosciences Press, Wuhan, p. 156.
Wignall, P.B., Sun, Y.D., Bond, D.P.G., Izon, G., Newton, R.J., Vedrine, S., Widdowson, M., Ali, J.R., Lai, X.L., Jiang, H.S., Cope, H., and Bottrell, S.H., 2009, Volcanism, mass extinction, and carbon isotope fluctuations in the Middle Permian of China. Science, v. 324, pp. 1179–1182.
Wu, Q., Ramezani, J., Zhang, H., Yuan, D.X., Erwin, D.H., Henderson, C.M., Lambert, L.L., Zhang, Y.C., and Shen, S.Z., 2020, High-precision U-Pb zircon age constraints on the Guadalupian in West Texas, USA. Palaeogeography, Palaeoclimatology, Palaeoecology, v. 548, pp. 109668.
Yang, J.H., Cawood, P.A., Du, Y.S., Condon, D.J., Yan, J.X., Liu, J.Z., Huang, Y., and Yuan, D.X., 2018, Early Wuchiapingian cooling linked to Emeishan basaltic weathering?. Earth and Planetary Science Letters, v. 492, pp. 102–111.
Yuan, D.X., Shen, S.Z., and Henderson, C.M., 2017, Revised Wuchiapingian conodont taxonomy and succession of South China. Journal of Paleontology, v. 91, pp. 1199–1219.
Yuan, D.X., Shen, S.Z., Henderson, C.M., Chen, J., Zhang, H., Zheng, Q.F., and Wu, H.C., 2019, Integrative timescale for the Lopingian (Late Permian): A review and update from Shangsi, South China. Earth-Science Reviews, v. 188, pp. 190–209.
Zhang, L.L., Zhang, N., and Xia, W.C., 2008, Conodont succession in the Guadalupian-Lopingian boundary interval (Upper Permian) of the Maoershan section, Hubei Province, China. Micropaleontology, v. 53, pp. 433–446.
Zhong, Y.T., He, B., Mundil, R., and Xu, Y.G., 2014, CA-TIMS zircon U–Pb dating of felsic ignimbrite from the Binchuan section: Implications for the termination age of Emeishan large igneous province, Lithos, v. 204, pp. 14–19.
Zhong, Y.T., He, B., and Xu, Y.G., 2013, Mineralogy and geochemistry of claystones from the Guadalupian–Lopingian boundary at Penglaitan, South China: Insights into the pre-Lopingian geological events. Journal of Asian Earth Sciences, v. 62, pp. 438–462.
Zhou, Z.R., 2017, Permian basinal ammonoid sequence in Nanpanjiang area of South China—possible overlap between basinal Guadalupian and platform-based Lopingian. Journal of Paleontology, Memoir 74, v. 91, pp. 1–95.

Shu-zhong Shen is a Professor at the School of Earth Sciences and Engineering of Nanjing University and a Member of Chinese Academy of Sciences. He was the former Chair of the Subcommission on Permian Stratigraphy and the current Vice-Chair of the International Commission on Stratigraphy. His main research interests include Permian brachiopods, conodonts, biostratigraphy, diversity patterns, end-Permian mass extinction and environmental changes in deep time.

Charles M. Henderson is a Professor at the University of Calgary where he has taught stratigraphy and paleontology since 1989. His research focusses on global biostratigraphy of Permian and Early Triassic conodonts and completing the chronostratigraphic subdivisions of the Permian System. He is a Fellow of The Royal Canadian Geographical Society and the Geological Society of America and former Chairman of the Subcommission on Permian Stratigraphy, ICS.

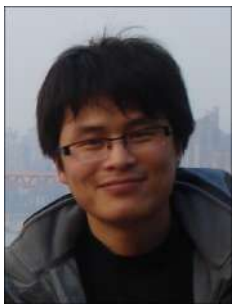

Dong-xun Yuan is an Associate Professor at the School of Resources and Geosciences, China University of Mining and Technology. He got his Ph.D. in geology of Nanjing University in 2015. His primary research focuses on the Permian conodonts, biostratigraphy, paleobiogeography and global correlation.

Quan-feng Zheng is an Associate Professor at the Nanjing Institute of Geology and Palaeontology, Chinese Academy of Sciences. His research mainly focuses on sedimentology and Permian stratigraphy.

Yi-chun Zhang is a Professor in the Nanjing Institute of Geology and Palaeontology, Chinese Academy of Sciences. He is the present secretary of Subcommission on Permian Stratigraphy. His research interests include taxonomy, biostratigrapy and paleobiogeography of Permian foraminifers and paleogeographic reconstructions of the Tethys region.

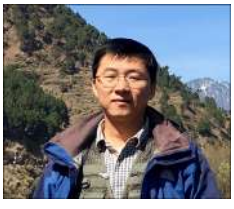

Hua Zhang is a Professor at the Nanjing Institute of Geology and Palaeontology, Chinese Academy of Sciences. His research interests include the end-Permian mass extinction, biogeochemistry and palaeoenvironmental changes in deep time.

Min Zhang is a postdoctoral at the Institute of Geology and Geophysics, Chinese Academy of Sciences. He got his Ph.D. in Geology from the University of Chinese Academy of Sciences in 2022. His main researches focus on the magnetostratigraphy of marine carbonate rocks and its implications for environmental and biological changes in deep time.

Yu Dai is a senior engineer at the Guangxi Institute of Regional Geological Survey. His main researches focus on the Tethys structure and mineralization, tin mineralization regularity, paleontology and geological heritages.

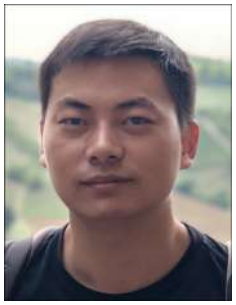

Hai-peng Xu is a postdoctoral research fellow at the School of Earth Sciences and Engineering of Nanjing University. He got his Ph.D. in Geology from Nanjing University in 2022. His main research interests include taxonomy, biostratigraphy and palaeobiogeography of Permian brachiopods from the Qinghai-Tibetan Plateau and surrounding areas.

Wen-qian Wang is a Assistant Professor at the School of Earth Sciences and Engineering of Nanjing University. Her current research interest is mainly on palaeoenvironment and palaeoclimate using geochemical proxies of brachiopod shells and conodonts.

Qian Li is a senior engineer of the search group of Geology and Mineral Resources of the Institute of Guangxi Regional Geological Survey. He graduated from the Guilin University of Technology with a bachelor's degree of resource exploration engineering. His primary research focuses on the regional geological (mineral) survey.

Yue Wang is a Professor at the Nanjing Institute of Geology and Palaeontology, Chinese Academy of Sciences. Her current research interests include the Permian stratigraphy, the systematics and evolution of Fusulinida, and the environmental and biological responses to the climatic transition from icehouse to greenhouse during the Early Permian.

Xiang-dong Wang is a Professor at the School of Earth Sciences and Engineering of Nanjing University. His research focuses on the Carboniferous and Permian stratigraphy, rugose corals, and the Late Paleozoic Ice Age. He is the current Chairman of the Subcommission on Carboniferous Stratigraphy.

Lin Mu is a Research Assistant of geology and paleontology at the Nanjing Institute of Geology and Palaeontology, Chinese Academy of Sciences. His research interests include the Paleozoic and Mesozoic ammonoids and their paleoecology, functional morphology and paleogeography.

Jahan Ramezani is a Research Scientist at the Massachusetts Institute of Technology. His research focuses on the high-precision U-Pb geochronology applied to the stratigraphic record and geologic history. His research focuses on calibration of the geologic time scale and co-evolution of Earth and life in deep time.

Douglas Erwin is a Senior Scientist in the Department of Paleobiology at the National Museum of Natural History of the Smithsonian Institution in Washington, DC, USA and external faculty at the Santa Fe Institute. His research interests include the rate, timing and nature of the end-Permian mass extinction; the early evolution of animals; and evolutionary novelty and innovation.

Lucia Angiolini is a Professor at the University of Milano, Italy where she has taught paleontology, palaeocology and biomineralization for more than 20 years. Her primary research is on the taxonomy and biostratigraphy of Carboniferous and Permian brachiopods and their paleoclimatological and paleoecological implications. She is the current Chairman of the Subcommission on Permian Stratigraphy, Vice-Director of the Department of Earth Sciences of the University of Milano, and the former President of the Società Paleontologica Italiana.

Fei-fei Zhang is a professor of isotope geochemistry and historical geobiology at the School of Earth Sciences and Engineering, Nanjing University. He received his Ph.D. in geological science at Arizona State University in 2018. His main research interests include developing and applying metal stable isotopes in studies of paleoceanographic and paleoenvironmental changes, the causes and consequences of climate extremes in Earth's history, the causes of major biological innovations and extinctions, and the coupling of geochemical proxy data and Earth system models.

Zhang-shuai Hou is a PhD candidate at the School of Earth Sciences and Engineering of Nanjing University. His primary research focuses on the Carboniferous and Permian ash beds and geochronological constraints on critical geological and biological events in deep time.

Jun Chen is an assistant research professor at the Guangzhou Institute of Geochemistry, Chinese Academy of Sciences (GIGCAS). His current research includes conodont biostratigraphy, palaeotemperature reconstruction using conodont apatite, and environmental and biological impact of large igneous provinces.

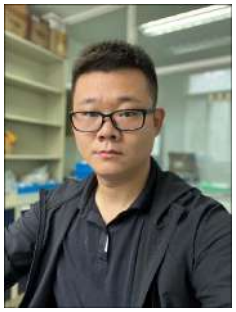

Xi-yang Zhang is an assistant research fellow at the South China Sea institute of Oceanology, CAS. He got his Ph.D. in geology of Nanjing institute of geology and palaeontology, CAS in 2019. His specializes in the anachronistic facies near the Permian-Triassic boundary.

Shu-han Zhang is a PhD student at the School of Earth Sciences and Engineering of Nanjing University. His primary research focus on quantitative stratigraphy, macroevolution and data analysis in paleobiology.

Qiong Wu is a research scientist at the Southern Marine Science and Engineering Guangdong Laboratory (Guangzhou). Her research interest includes the application of high-precision U-Pb geochronology by LA-ICPMS, SIMS and CA-ID-TIMS techniques to chronostratigraphy of marine and terrestrial sediments and calibration of various geological and biological events.

Yong-xin Pan is a Professor at the Institute of Geology and Geophysics, Chinese Academy of Sciences, Beijing. He is the founding director of Biogeomagnetism Laboratory. His research interests include the linkage between life and geomagnetic field, variations of geomagnetic field, magnetostratigraphy, mineral magnetism, biomineralization and applications, magnetic field of Mars.

Michael H. Stephenson is Executive Chief Scientist and professor (Decarbonisation) at the British Geological Survey. He has done research in the Middle East and Asia, including in Oman, Saudi Arabia, Jordan, Pakistan, Iran, Israel and Iraq. He has professorships at Nottingham and Leicester universities in the UK and is a visiting professor at the University of Nanjing, China. He has published three books and over 100 peer-reviewed papers. His recent book 'Energy and Climate Change: An Introduction to Geological Controls, Interventions and Mitigations' examines the Earth system science of the formation and use of fossil fuel resources, and the implications for climate change.

Shi-long Mei is currently a senior geologist of Alberta Geological Survey (AGS) in Canada. Prior to joining AGS in 2003, he worked and published on Devonian Archaeopteris, Cambrian inarticulate brachiopods, Cambrian, Ordovician, Permian and basal Triassic conodonts, and global correlation of Permian and basal Triassic conodont biostratigraphy.

Appendices: Descriptions of the Studied Sections

Appendix 1: Description of the new GSSP section at Penglaitan (Figs. 1, 2)

Heshan Formation

Unit n7. Black thin- to medium-bedded chert with multiple volcanic ash beds, 3.3 m (11.7-14.0 m)

Bed n7j, black medium-bedded chert, yielding conodont *Clarkina dukouensis*, 1.28 m (12.72-14.0 m).

Bed n7i, volcanic ash, 2 cm (12.70-12.72 m).

Bed n7h, brownish chert, 6 cm (12.64-12.70 m).

Bed n7g, greenish volcanic ash, 4 cm (12.60-12.64 m).

Bed n7f, dark grey medium-bedded chert with limestone lenses, 28 cm (12.32-12.60 m).

Bed n7e, greenish volcanic ash, 2 cm (12.3-12.32 m).

Bed n7d, dark grey medium-bedded chert, fragile, yielding conodont *Clarkina dukouensis*, 35 cm (11.95-12.3 m).

Bed n7c, greenish volcanic ash, 5 cm (11.90-11.95 m).

Bed n7b, black thin-bedded chert with limestone lenses, fragile, yielding abundant conodont *Clarkina postbitteri*, 10 cm (11.80-11.90 m).

Bed n7a, greenish volcanic ash bed, 10 cm (11.70-11.80 m).

——————————conformity——————————

Maokou Formation (Laibin Limestone)

Unit n6. Coarse dark grey medium-bedded crinoid limestone containing tuffaceous materials, 2.07 m (9.63-11.70 m).

Bed n6m, coarse dark grey medium-bedded crinoid limestone, yielding conodont *Clarkina postbitteri* and transitional forms to *Jinogondolella granti*. 15 cm (11.56-11.70 m).

Bed n6L, coarse dark grey medium-bedded crinoid limestone, yielding conodont *Clarkina postbitteri* and *Jinogondolella granti*, 21 cm (11.35-11.56 m). The base of this bed has been defined as the new GSSP at Penglaitan.

Bed n6k, coarse dark grey medium-bedded crinoid limestone containing tuffaceous materials, yielding abundant conodont *Jinogondolella granti* and the solitary corals *Cania*, 29 cm (11.06-11.35 m).

Bed n6j, coarse dark grey medium-bedded crinoid limestone containing tuffaceous materials and the conodont *Jinogondolella granti*, 11 cm (10.95-11.06 m).

Bed n6i, coarse dark grey medium-bedded crinoid limestone containing tuffaceous materials, 20 cm (10.75-10.95 m).

Bed n6h, coarse dark grey medium-bedded crinoid limestone containing tuffaceous materials, 16 cm (10.59-10.75 m).

Bed n6g, coarse dark grey medium-bedded crinoid limestone containing tuffaceous materials, 22 cm (10.43-10.59 m).

Bed n6f, coarse dark grey medium-bedded crinoid limestone containing tuffaceous materials, 12 cm (10.31-10.43 m).

Bed n6e, coarse dark grey medium-bedded crinoid limestone containing tuffaceous materials, 11 cm, (10.20-10.31 m).

Bed n6d, dark grey medium-bedded crinoid limestone, 14 cm, (10.06-10.20 m)

Bed n6c, ash bed, 6 cm, (10.00-10.06 m).

Bed n6b, dark grey thin-bedded limestone with cross-bedding, yielding the conodont *Jinogondolella granti,* 10 cm, (9.90-10.00 m).

Bed n6a, Dark grey medium-bedded crinoid limestone with cross-bedding, 27 cm (9.63-9.90 m).

Unit n5. Medium-bedded limestone with tuffaceous materials, 85 cm (8.78-9.63 m).

Bed n5e, ash bed, 3 cm (9.60-9.63 m).

Bed n5d, dark grey thin-bedded limestone containing abundant tuffaceous materials, 8 cm (9.52-9.60 m).

Bed n5c, dark grey thick-bedded limestone containing volcanic materials, limestone breccia, abundant brachiopods, corals *Cania* and the conodont *Jinogondolella granti*, 35 cm (9.18-9.53).

Bed n5b, dark cherty limestone with 3 cm ash bed at the base, containing brachiopods *Spinomarginifera lopingensis*, 18 cm (9.0-9.18 m).

Bed n5a, dark grey medium-bedded limestone containing the brachiopod *Spinomarginifera lopingensis*, the conodont *Jinogondolella granti*, ammonoids and corals, 22cm (8.78-9.0 m).

Unit n4. Dark grey medium-bedded crinoid limestone, 1.48 m (7.3-8.78 m).

Bed n4k, dark grey medium-bedded crinoid limestone, 11 cm (8.67-8.78 m).

Bed n4j, dark grey medium-bedded crinoid limestone with thin cherty bands, containing abundant nautiloids and conodont *Jinogondolella granti*, 15 cm (8.52-8.67 m).

Bed n4i, dark grey medium-bedded crinoid limestone, containing abundant conodont *Jinogondolella granti*, 11 cm (8.41-8.52 m).

Bed n4h, dark grey medium-bedded or lenticular crinoid limestone, containing abundant conodont *Jinogondolella granti*, 11cm (8.3-8.41 m).

Bed n4g, dark grey thin-bedded or lenticular crinoid limestone, 5 cm (8.25-8.30 m).

Bed n4f, dark grey medium-bedded crinoid limestone, containing abundant conodont *Jinogondolella granti*, 25 cm (8.0-8.25 m).

Bed n4e, dark grey medium-bedded crinoid limestone, containing abundant conodont *Jinogondolella granti*, 13 cm (7.87-8.0 m).

Bed n4d, dark grey medium-bedded crinoid limestone, containing abundant conodont *Jinogondolella granti*, 12 cm (7.65-7.87 m).

Bed n4c, dark grey medium-bedded crinoid limestone, containing abundant conodont *Jinogondolella granti*, 14 cm (7.51-7.65 m).

Bed n4b, dark grey medium-bedded limestone, containing some reddish breccia and abundant crinoid fragments and abundant conodont *Jinogondolella granti*, bedding plane corrugated, 13 cm (7.38-7.51 m).

Bed n4a, dark grey thin-bedded limestone with cherty bands, containing abundant crinoids and conodont *Jinogondolella granti*, 8 cm (7.30-7.38 m).

Unit n3. Pale grey thick-bedded limestone containing abundant brachiopods including *Spinomarginifera lopingensis*. 2.95 m (4.35-7.30 m).

Unit n2. Greyish thin- to medium-bedded limestone with chert bands along the bedding plane, 0.94 cm (3.41-4.35 m).

Unit n1. Mostly covered

Appendix 2: Description of the SABS at Fengshan (Fig. 4)

The section is measured about 87 m in thickness and every metre is marked with paint on the outcrop. Limestone beds are dominant and 33 lithological units have been identified, with some units subdivided into several subunits. Samples of conodonts, fusulines and brachiopods and other fossils were collected from this section. More than 130

samples with an average weight between 5-20 kg have been collected from each limestone bed across the GLB.

Lower part of Lopingian Heshan Formation (18.5 m thick in total)

Unit 32. Dark grey to greyish, thin- to medium-bedded, bioclastic wackestone and lime mudstone, intercalated with thin-bedded bioclastic packstone, yielding conodont *Clarkina guangyuanensis*, *Hindeodus julfensis*, *H.* sp., *Merrilina divergens*; and fusuline *Reichelina changhsingensis*. 8.3 m (72.5 m-80.8 m).

Unit 31. Pale grey to greyish thick-bedded rudstone and floatstone containing fusuline *Reichelina changhsingensis*. 0.75 m (71.75 m-72.5 m).

Unit 30. Dark to pale grey, thin- to medium-bedded, bioclastic packstone or wackestone with cherty nodules and bands. Containing conodont *Clarkina asymmertica*, *Hindeodus julfensis*, *H.* sp.; and fusuline *Reichelina changhsingensis*. 2.4 m (69.35 m-71.75 m).

Unit 29. Dark grey to greyish, thin- to medium-bedded bioclastic packstone, wackestone and lime mudstone with cherty-nodules, yielding conodont *Clarkina dukouensis*, *Hindeodus julfensis*, *H*. sp., *Iranognathus* sp.; and fusuline *Reichelina changhsingensis*. 4.7 m (64.65 m-69.35 m).

Unit 28. Dark grey to greyish, medium-bedded wackestone and lime mudstone, yielding conodont *Clarkina postbitteri*, *C. dukouensis*, *Hindeodus* sp. and *Iranognathus* sp. 2.15 m (62.5 m-64.65 m). This unit has been further subdivided into 9 subunits.

28-9. Dark grey, thin- to medium-bedded, bioclastic wackestone-lime mudstone, yielding the conodont *Clarkina dukouensis*. 0.3 m (64.35 m-64.65 m);

28-8. Dark grey, thin- to medium-bedded, bioclastic packstone-wackestone, yielding the conodonts *Clarkina dukouensis*, *Iranognathus* sp., *Hindeodus* sp. 0.94 m (63.41 m-64.35 m);

28-7. Dark grey, medium-bedded, bioclastic wackestone-lime mudstone, yielding the conodonts *Clarkina dukouensis*, *Hindeodus* sp. 0.2 m (63.21 m-63.41 m);

28-6. Dark grey, lenticular, bioclastic packstone-wackestone. 0.05 m (63.16 m-63.21 m);

28-5. Dark grey, medium-bedded, bioclastic wackestone-lime mudstone, yielding the conodonts *Clarkina dukouensis*, *C. postbitteri*, *Hindeodus* sp. 0.18 m (62.98 m-63.16 m);

28-4. Dark grey, lenticular, bioclastic packstone-wackestone. 0.04 m (62.94 m-62.98 m);

28-3. Dark grey, medium-bedded, bioclastic wackestone-lime mudstone, yielding the conodonts *Clarkina postbitteri*, *Hindeodus* sp. 0.11 m (62.83 m-62.94 m);

28-2. Dark grey, lenticular, bioclastic packstone-wackestone. 0.08 m (62.75 m-62.83 m);

28-1. Dark grey, medium-bedded, bioclastic wackestone-lime mudstone, yielding the conodonts *Clarkina postbitteri*, *Hindeodus* sp., *Iranognathus* sp. 0.25 m (62.5 m-62.75 m);

Unit 27. Grey medium-bedded bioclastic grainstone, pinching out laterally, it may contain an ash bed within it. 0.2 m (62.3 m-62.5 m).

——————————conformity——————————

Upper part of Maokou Formation (68.6 m in total)

Unit 26. Grey to dark grey, bedded to nodular bioclastic packstone, wackestone and grainstone, yielding conodont *Clarkina postbitteri*, *Jinogondolella granti*, *J. xuanhanensis*, *Sweetognathus fengshanensis*, *Hindeodus* sp. and fusuline *Reichelina changhsingensis*, *R. simplex* and *Lantschichites minima*. 1.2 m (61.1 m-62.3 m). This unit is subdivided into three subunits:

26-3. Grey to dark grey, nodular, bioclastic packstone-wackestone, yielding the conodont *Clarkina postbitteri*, *Jinogondolella granti*, *Sweetognathus fengshanensis*, *Hindeodus* sp. 0.5 m (61.8 m -62.3 m). The Guadalupian/Lopingian boundary is correlated at 62.0 m in this bed, 30 cm below the top of Unit 26 (Fig. 8). The sample between 62.0-62.3 m contains both *Clarkina postbitteri* and *Jinogondolella granti*, and some transitional forms between these two species.

26-2. Dark grey bioclastic grainstone-rudstone, yielding *Jinogondolella* sp. 0.1 m (61.7 m-61.8 m);

26-1. Grey to dark grey, nodular, bioclastic packstone-wackestone, yielding the conodont *Jinogondolella granti*, transitional to *J. granti*, *J. xuanhanensis*, *Hindeodus* sp. 0.6 m (61.1 m-61.7 m).

Unit 25. Pale grey, medium-bedded bioclastic wackestone, packstone and grainstone yielding conodont *Jinogondolella granti*, transitional to *J. granti*, *J. xuanhanensis*, *Hindeodus* sp.; fusuline *Chenella changanchiaoensis*, *Codonofusiella extensa*, *C. paradoxica*, *Kahlerina pachytheca*, *Lantschichites minima*, *Rauserella erratica*, *Reichelina changhsingensis*, *R. simplex.* 1.6 m (59.5 m-61.1 m). This unit is subdivided into 8 subunits.

25-8. Pale grey medium-bedded bioclastic grainstone-rudstone, yielding the conodonts *Jinogondolella granti*, *Hindeodus* sp. 0.2 m (60.90 m-61.10 m);

25-7. Pale to dark grey, nodular, bioclastic packstone, wackestone or lime mudstone, yielding the conodonts *Jinogondolella xuanhanensis*, transitional to *Jinogondolella granti*. 0.25 m (60.65 m-60.90 m);

25-6b. Pale grey medium-bedded bioclastic grainstone-rudstone, yielding the conodonts *Hindeodus* sp., transitional to *Jinogondolella granti*. 0.2 m (60.45 m-60.65 m);

25-6a. Pale grey sponge-brachiopod floatstone. 0.1 m (60.35 m-60.45 m);

25-5. Pale to dark grey, nodular, bioclastic wackestone-lime mudstone, yielding the conodont *Jinogondolella xuanhanensis*. 0.1 m (60.25 m-60.35 m);

25-4. Pale to dark grey, nodular, bioclastic wackestone-lime mudstone, yielding the conodonts *Hindeodus* sp., transitional to *Jinogondolella granti*. 0.25 m (60.0 m-60.25 m);

25-3. Grey to pale grey, medium-bedded, bioclastic wackestone, packstone or grainstone, yielding the conodont *Jinogondolella* sp. 0.3 m (59.7 m-60.0 m);

25-2. Pale grey nodular bioclastic wackestone. 0.05 m (59.65 m-59.7 m);

25-1. Pale grey, medium-bedded, bioclastic grainstone-rudstone. 0.15 m (59.5 m-59.65 m).

Unit 24. Dark reddish, grey, thick- to very thick-bedded and massive reef limestone yielding conodont *Jinogondolella xuanhanensis*, transitional to *J. granti*, *Sweetognathus fengshanensis*; and fusuline *Chenella changanchiaoensis*, *Codonofusiella schubertelloides*, *C. paradoxica*, *C. extensa*, *Kahlerina pachytheca*, *Lantschichites minima*, *Reichelina simplex, Nankinella nanjingensis*, *Rauserella erratica*, *Schwagerina serrata*, *Metadoliolina multivoluta*, *M. douvillei*. 1.9 m (57.6 m-59.5 m).

Unit 23. Pale grey to greyish, very thick-bedded, bioclastic pack-

stone, grainstone and rudstone yielding conodont *Jinogondolella xuanhanensis*, transitional to *J. granti*, *Sweetognathus fengshanensis*, *Hindeodus* sp.; fusuline *Reichelina changhsingensis*, *R. simplex*, *Lantschichites minima*, *Kahlerina pachytheca*, *K. sinensis*, *Codonofusiella paradoxica*, *C. schubertelloides*, *Chenella changanchiaoensis*, *Rauserella erratica*, *Metadoliolina multivoluta*, *M. douvillei*, *M. delicata*, *Schwagerina serrata*, *Nankinella nanjingensis*, *Chusenella douvillei*, *C. globularis*, *Neoschwagerina* sp.; and brachiopods *Alphaneospirifer pyramidiformis*, *Juxathryis guizhouensis, Enteletes kayseri*, *Martinia* sp. 29.9 m (27.7 m-57.6 m).

Unit 22. Dark reddish grey, very thick-bedded, reef limestone yielding conodont *Jinogondolella xuanhanensis*, *Sweetognathus fengshanensis*, *Hindeodus* sp.; fusuline *Chenella changanchiaoensis*, *Lantschichites minima*, *Kahlerina pachytheca*; and brachiopod *Urushtenoidea crenulata*, *Martinia* sp., *Juxathyris guizhouensis*, *Juxathyris* sp., *Uncinunellina timorensis*, *Permophricodothyris* sp. 9.8 m (17.9 m-27.7 m).

Unit 21. Pale grey, very thick-bedded, bioclastic and lithoclastic rudstone containing conodont *Jinogondolella xuanhanensis*; and fusuline *Lantschichites minima*, *Reichelina changhsingensis*, *Rauserella erratica* and brachiopods *Permophiricodothyris elegantula*, *Alphaneospirifer* sp., *Juxathyris* sp., *Spinomarginifera* sp., *Enteletes* sp., *Zhejiangospirifer abnormalis*. 2.8 m (15.1 m-17.9 m).

Unit 20. Pale to dark grey, nodular, bioclastic wackestone-lime mudstone. 0.25 m (14.85 m-15.1 m).

Unit 19. Pale grey medium-bedded bioclastic grainstone. 0.3 m (14.55 m-14.85 m).

Unit 18. Grey to dark grey, nodular, bioclastic packstone, wackestone and lime mudstone yielding conodont *Sweetognathus fengshanensis* and *Jinogondolella xuanhanensis*. 0.3 m (14.25 m-14.55 m).

Unit 17. Pale grey, medium- to very thick-bedded, bioclastic grainstone yielding conodont *Jinogondolella xuanhanensis* and fusuline *Schwagerina serrata*. 1.55 m (12.7 m-14.25 m).

Unit 16. Pale to dark grey, nodular, bioclastic wackestone and lime mudstone yielding conodont transitional to *Jinogondolella xuanhanensis*. 0.15 m (12.55 m-12.7 m).

Unit 15. Pale grey, thin-bedded, bioclastic grainstone. 0.1 m (12.45 m-12.55 m).

Unit 14. Pale to dark grey, nodular, bioclastic packstone, wackestone and lime mudstone yielding conodont transitional to *Jinogondolella xuanhanensis*. 0.2 m (12.25 m-12.45 m).

Unit 13. Pale grey, medium- to thick-bedded, bioclastic grainstone. 0.3 m (11.95 m-12.25 m).

Unit 12. Grey to pale grey, nodular, bioclastic wackestone and lime mudstone yielding conodont *Sweetognathus fengshanensis*, transitional to *Jinogondolella xuanhanensis*. 0.25 m (11.7 m-11.95 m).

Unit 11. Pale grey, medium- to thick-bedded, bioclastic grainstone yielding fusuline *Metadoliolina multivoluta*, *M. douvillei*. 0.8 m (10.9 m-11.7 m).

Unit 10. Grey to pale grey, bioclastic wackestone, lime mudstone and rudstone yielding conodont *Sweetognathus fengshanensis*, transitional to *Jinogondolella xuanhanensis*. 0.15 m (10.75 m-10.9 m).

Unit 9. Pale grey, medium- to thick-bedded, bioclastic grainstone. 0.35 m (10.4 m-10.75 m).

Unit 8. Grey to dark grey, nodular, bioclastic packstone, wackestone and lime mudstone. 0.2 m (10.2 m-10.4 m).

Unit 7. Pale grey, medium- to thick-bedded, bioclastic grainstone yielding conodont transitional to *Jinogondolella xuanhanensis*. 0.7 m (9.5 m-10.2 m).

Unit 6. Grey to dark grey, nodular, bioclastic wackestone and lime mudstone. 0.1 m (9.4 m-9.5 m).

Unit 5. Pale grey, medium- to thick-bedded, bioclastic grainstone yielding conodont *Sweetognathus fengshanensis*, transitional to *Jinogondolella xuanhanensis*. 0.7 m (8.7 m-9.4 m).

Unit 4. Dark grey nodular bioclastic wackestone. 0.05 m (8.65 m-8.7 m).

Unit 3. Pale grey to greyish, thin- to thick-bedded, bioclastic wackestone, packstone and grainstone yielding conodont *Sweetognathus fengshanensis*, transitional to *Jinogondolella xuanhanensis*; and fusuline *Schwagerina serrata*, *Metadoliolina multivoluta*, *Kahlerina pachytheca*. 6.95 m (1.7 m-8.65 m).

Unit 2. Pale grey to greyish, medium- to thick-bedded, bioclast-lichoclast rudstone. 1.15 m (0.55 m-1.7 m).

Unit 1. Pale grey, thick-bedded, bioclast-lichoclast rudstone yielding conodont *Sweetognathus* sp., transitional to *Jinogondolella xuanhanensis*. 0.55 m (0 m-0.55 m).

Unit 0-1. Dark grey, thin- to medium-bedded, bioclastic wackestone containing cherty nodules yielding conodont *Sweetognathus* sp. and transitional to *Jinogondolella xuanhanensis*. 4.2 m (-4.2 m-0 m).

Unit 0-2. Dark grey, thin- to medium-bedded, bioclastic wackestone and packstone alternating with dark to dark grey, thin-bedded cherts yielding conodonts: transitional to *Jinogondolella xuanhanensis*. 2.1 m (-4.2 m to -6.3 m).